

Original citation:

Ahmadi, Ehsan, Caprani, Colin, Živanović, Stana, Evans, Neil D. and Heidarpour, Amin (2018) A framework for quantification of human-structure interaction in vertical direction. Journal of Sound and Vibration, 432 . pp. 351-372. doi:10.1016/j.jsv.2018.06.054

Permanent WRAP URL:

<http://wrap.warwick.ac.uk/103971>

Copyright and reuse:

The Warwick Research Archive Portal (WRAP) makes this work by researchers of the University of Warwick available open access under the following conditions. Copyright © and all moral rights to the version of the paper presented here belong to the individual author(s) and/or other copyright owners. To the extent reasonable and practicable the material made available in WRAP has been checked for eligibility before being made available.

Copies of full items can be used for personal research or study, educational, or not-for-profit purposes without prior permission or charge. Provided that the authors, title and full bibliographic details are credited, a hyperlink and/or URL is given for the original metadata page and the content is not changed in any way.

Publisher's statement:

© 2018, Elsevier. Licensed under the Creative Commons Attribution-NonCommercial-NoDerivatives 4.0 International <http://creativecommons.org/licenses/by-nc-nd/4.0/>

A note on versions:

The version presented here may differ from the published version or, version of record, if you wish to cite this item you are advised to consult the publisher's version. Please see the 'permanent WRAP url' above for details on accessing the published version and note that access may require a subscription.

For more information, please contact the WRAP Team at: wrap@warwick.ac.uk

1 **A Framework for Quantification of Human-Structure Interaction** 2 **in Vertical Direction**

3 Ehsan Ahmadi¹, Colin Caprani^{1*}, Stana Živanović², Neil Evans², Amin Heidarpour¹

4 ¹ Dept. of Civil Engineering, Monash University, Australia

5 ² School of Engineering, University of Warwick, UK

6 * Corresponding Author

7 8 9 10 11 **Abstract**

13 In lightweight structures, there is increasing evidence of the existence of interaction between
14 pedestrians and structures, now commonly termed pedestrian-structure interaction. The
15 presence of a walker can alter the dynamic characteristics of the human-structure system
16 compared with those inherent to the empty structure. Conversely, the response of the structure
17 can influence human behaviour and hence alter the applied loading. In the past, most effort on
18 determining the imparted footfall-induced vertical forces to the walking surface has been
19 conducted using rigid, non-flexible surfaces such as treadmills. However, should the walking
20 surface be vibrating, the characteristics of human walking could change to maximize comfort.
21 Knowledge of pedestrian-structure interaction effects is currently limited, and it is often quoted
22 as a reason for our inability to predict vibration response accurately. This work aims to quantify
23 the magnitude of human-structure interaction through a experimental-numerical programme
24 on a full-scale lively footbridge. An insole pressure measurement system was used to measure
25 the human-imparted force on both rigid and lively surfaces. Test subjects, walking at different
26 pacing frequencies, took part in the test programme to infer the existence of the two forms of
27 human-structure interaction. Parametric statistical hypothesis testing provides evidence on the
28 existence of human-structure interaction. In addition, a non-parametric test (Monte Carlo
29 simulation) is employed to quantify the effects of numerical model error on the identified
30 human-structure interaction forms. It is concluded that human-structure interaction is an

31 important phenomenon that should be considered in the design and assessment of vibration-
32 sensitive structures.

33

34 **Keywords**

35 Human-structure interaction; footbridge vibration; experiment; in-sole sensors

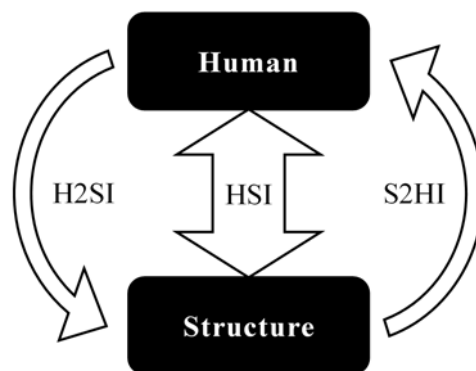
36

37 **1. Introduction**

38 Many newly built structures have light weight, low damping, and low stiffness, and they may
39 not satisfy vibration serviceability criteria when occupied and dynamically excited by humans
40 [1]. Observed problems have been caused typically by human occupants performing normal
41 activities such as walking, running, jumping, bouncing/bobbing, and dancing. Vibration
42 beyond the human comfort range will influence human comfort and so is a key consideration
43 for designers. Human presence can affect the dynamic characteristics of the coupled human-
44 structure system during motion, named here as Human-to-Structure Interaction (H2SI). On the
45 other hand, the vibrating structure may change the human activity force pattern, and this
46 potential phenomenon is named here as a Structure-to-Human Interaction (S2HI) (Figure 1).
47 These postulated mutual effects between human and structure are collectively referred to as
48 human-structure interaction (HSI). Since for this work we consider only single human loading
49 situations, we do not consider human-to-human interaction which can take place in crowds.
50 The H2SI and S2HI effects are usually considered mutually exclusive [2], meaning that HSI is
51 often modelled through a change in the dynamic properties of the system only or a change in
52 walking force only. In this study, they are assumed to be mutually independent, isolated and
53 examined individually using a novel experimental-numerical programme while both types
54 occur simultaneously.

55

56 The focus of this study is on human walking and the resulting vibration. To assess the vibration
57 response of structures susceptible to human walking, accurate estimation of human force,
58 dynamic characteristics of the structure, and human-structure interaction are required
59 (Figure 1). As a novel aspect of this work, human walking force was measured using TekScan
60 F-scan in-shoe plantar pressure sensors intended for medical applications. The plantar pressure
61 force gives a reliable measurement of the vertical walking force [3], [4]. Further, the mass,
62 damping, and stiffness of the structure were obtained using system identification methods. The
63 most challenging part of the study of human-structure interaction is to identify and quantify the
64 postulated forms of HSI separately. This study proposes an experimental framework to address
65 this challenge. It relies on acquiring sufficiently accurate measurements of the human force,
66 structure dynamics, and comparison of data recorded on rigid and flexible surfaces. The two
67 postulated forms of HSI will be described in more detail in the next two sections.



68 Figure 1 Interactions between humans and the structure in the human-structure system are collectively called
69 Human-Structure Interaction (HSI), but are considered separately here as Human-to-Structure Interaction
70 (H2SI) and Structure-to-Human Interaction (S2HI).
71
72

73 The human body is a sensitive vibration receiver characterized by an innate ability to adapt
74 quickly to almost any type and level of vibration which normally occurs in nature [5]. This
75 effective self-adapting mechanism triggers pedestrians to change their walking behaviour [6].
76 In turn, it leads to walking force patterns that can be different to those measured on non-
77 vibrating rigid surfaces [7].

78

79 There have been numerous attempts to measure or model pedestrian-induced forces, referred
80 to as ground reaction forces (GRFs); see for example [8], [9], [10], [11], [12], [13], [14]. Past
81 GRF measurement facilities typically comprised equipment for direct force measurements,
82 such as a force plate [15], or an instrumented treadmill usually mounted on rigid laboratory
83 floors ([16], [17], [18]). However, GRFs could differ when walking on vibrating surface. For
84 example, Ohlsson [19] found that the vertical force measured on a flexible timber floor is
85 different from that measured on a rigid base. Pavic et al. [20] pointed out that the force induced
86 by jumping on a flexible concrete beam was lower than that on a force plate. Van Nimmen et
87 al. [21] and Bocian et al. [22] indirectly reconstructed vertical walking force on bridge surfaces
88 from inertial motion tracking and a single point inertial measurement respectively. To the
89 authors' knowledge, Dang and Zivanovic [23] is the only experimental work on direct
90 measurement of walking GRFs on lively structures in the vertical direction. The results showed
91 a drop in the first dynamic load factor of the walking force due to the bridge vibration at the
92 resonance. However, test subjects walked on-the-spot on a treadmill for this study.

93
94 Humans add mass, stiffness, and damping to the coupled human-structure system. The
95 influence of passive humans on the dynamic properties of the structure they occupy (i.e. modal
96 mass, damping, and stiffness) have been well-documented in the literature [24], [2], [25], [26].
97 For example, Ohlsson [19] found that a walking pedestrian can increase the HSI system's
98 frequency and damping, while Willford [27] also reported a change in the system's damping
99 due to moving crowd in the vertical direction. Zivanovic et al. [28] and Van Nimmen et al. [29]
100 identified modal properties of the HSI system and showed that the presence of humans on the
101 structure, either in standing or walking form, will increase the damping of the system compared
102 to the empty structure. Zivanovic et al. [30] revealed that crowd effects can be also modelled
103 as an increase in the damping of the system, in some cases more than two times greater than

104 the damping ratio for the empty bridge, and Caprani et al. [31] did so to account for crowd
105 damping effects. Kasperski [32] also concluded that a walking pedestrian can induce additional
106 damping by using discrete Fourier transform of the acceleration time history response of the
107 bridge. However, these existing effects are not incorporated into design codes and guidelines
108 such as OHBDC [33], U.K. National Annex to Eurocode 1 (British Standards Institution 2008)
109 [34], ISO-10137 [35], Eurocode 5 [36], Setra [37], and HIVOSS [38] as they model humans as
110 a moving force only. Interestingly, the U.K. National Annex to Eurocode 1 does acknowledge
111 that H2SI effects exist, but does not offer guidance on their inclusion, underlining the need to
112 quantify the H2SI effect on vibration.

113

114 The review above has shown that quantification of human-structure interaction is a crucial part
115 of vibration response estimation and that there is some evidence of the two postulated forms of
116 HSI in the literature. However, these HSI forms are not fully experimentally quantified, which
117 is an essential step towards the development of design/assessment guidelines that can consider
118 HSI. This work experimentally investigates the existence of the two postulated HSI forms by
119 isolating their influence on the vibration response. To this end, a novel experimental-numerical
120 programme is adopted. The human-imparted forces to both flexible (i.e. footbridge) and rigid
121 surfaces are measured. These are then used to simulate the vibration response. The simulated
122 vibration response from walking force measured on the rigid surface represents state-of-the-art
123 practice. The vibration response of the footbridge is also directly measured. Comparison of
124 dynamic load factors of the forces on the bridge surface with those of rigid surface should
125 reveal any walking pattern change due to HSI (S2HI). Another comparison for simulated
126 vibration responses due to the rigid and bridge surface walking forces discloses the effect of
127 S2HI on the vibration response. Comparing the simulated bridge vibration response and the
128 measured vibration response gives a good insight into the effects of HSI on the changes in

129 system dynamic characteristics (H2SI). A parametric statistical hypothesis test is then used to
130 show the generality of the results for a large number of walking trial scenarios. Finally, a non-
131 parametric test (Monte Carlo simulation) is conducted to determine the influence of model
132 errors on the two postulated forms of HSI. This experimental-numerical approach is next
133 described in detail.

134

135 **2. Experimental Procedure**

136 **2.1 Experimental-numerical programme**

137 Figure 2 schematically illustrates the experimental-numerical programme design to investigate
138 HSI. Two types of measurement are taken: (1) GRFs from walking on a rigid surface (RS), G_{RS}
139 (part (a) in Figure 2); (2) GRFs from walking on a vibrating bridge surface (BS), G_{BS} (part (b)),
140 while the vibration response of the bridge, R_M (part (f)), is concurrently measured. Subsequent
141 to these physical measurements, vibration responses to the measured RS and BS GRFs are
142 simulated using a system model (part (c)), namely a modal model of the bridge and a moving
143 force (MF) model of the pedestrian. These were denoted R_{RS} (part (d)), and R_{BS} (part (e)),
144 respectively.

145

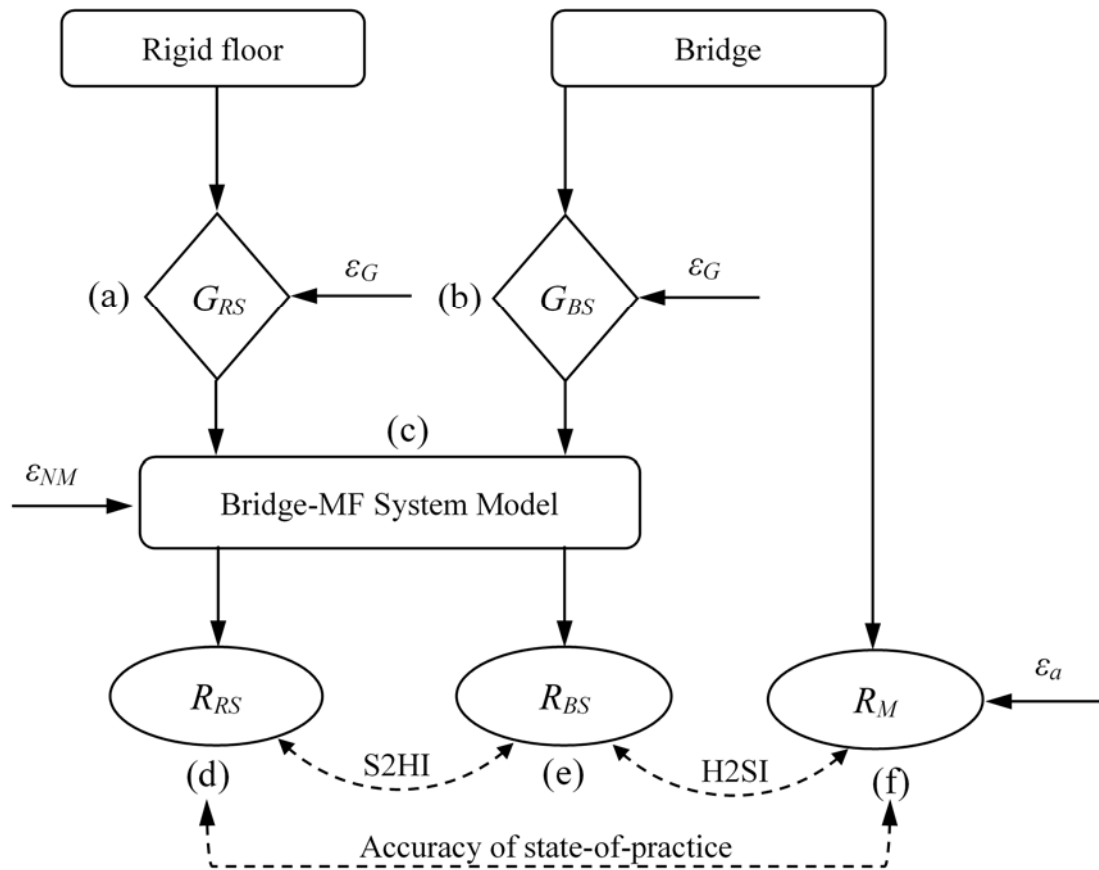


Figure 2 A schematic overview of the experimental-numerical programme, including an assessment of the accuracy of typical current practice using a moving force approach.

146
147
148
149

150 In this study, a difference between the vibration responses R_{RS} (part (d)) and R_{BS} (part (e)) of
151 the analytical model is considered as evidence of the influence of the vibrating bridge surface
152 on the walker-induced force (S2HI) (part (a) versus part (b)). Going a step farther, comparing
153 the simulated vibration response, R_{BS} , to those measured from the bridge, R_M , yields the
154 accuracy of the coupled bridge-MF system model (part (c)) itself. Here, there are two potential
155 errors to the system model: (1) the accuracy of the bridge model, and (2) the accuracy of MF
156 model due to H2SI. A reliable system identification method and using amplitude-dependent
157 frequency and damping of the bridge can significantly increase the accuracy of the bridge
158 model and reduce the first source of error in the system model to a very small amount.
159 Consequently, any difference between R_{BS} and R_M is because the MF model is unable to insert
160 human effects into the numerical model, H2SI. Further, comparison of R_{RS} and R_M implies the

161 accuracy of state-of-the-art design practice as the MF model and rigid surface force are used to
162 estimate the actual bridge response R_M .

163

164 The influence of errors in various measurements, ε , is also considered. The system numerical
165 model error, ε_{NM} , and measurement errors, ε_G and ε_a will be discussed later. Monte Carlo
166 simulations are performed to evaluate the influence of these errors (which are difficult to
167 measure) on the HSI quantifications.

168

169 **2.2 Walking trials**

170 All tests were carried out on the Warwick Footbridge – a steel-concrete composite laboratory
171 footbridge at the University of Warwick, UK, shown in Figure 3. The bridge is a unique
172 laboratory structure purpose-built with a natural frequency in the vertical direction that can be
173 matched by pacing rate, making it an ideal facility for studying HSI. The simply-supported
174 span length of the bridge is adjustable, but was kept constant throughout the tests at 16.2 m.
175 The bridge is 2 m wide, with a clear walkway track down the centre. The bridge mass is
176 approximately 16500 kg, and the modal mass of the first bending mode is 7614 kg with natural
177 frequency of about 2.43 Hz [39]. As a unique facility, it has already been used considerably for
178 the study of human-induced vibration [23].

179

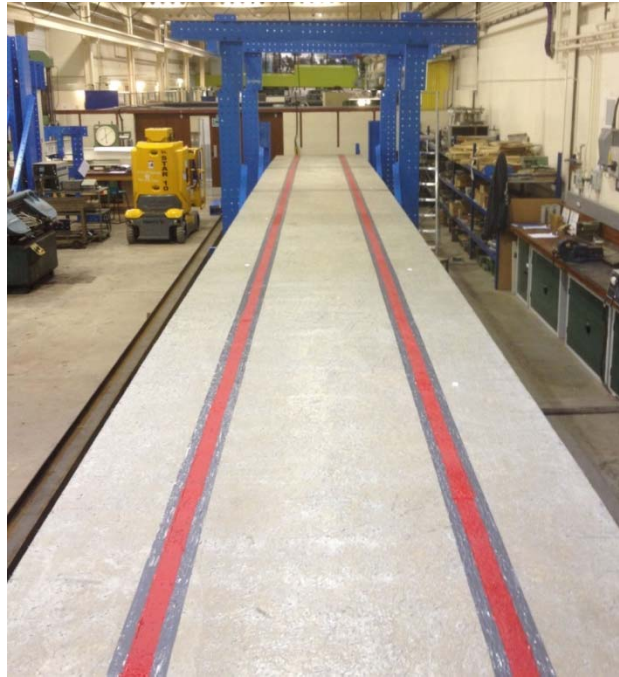


Figure 3 The Warwick footbridge.

180
181
182

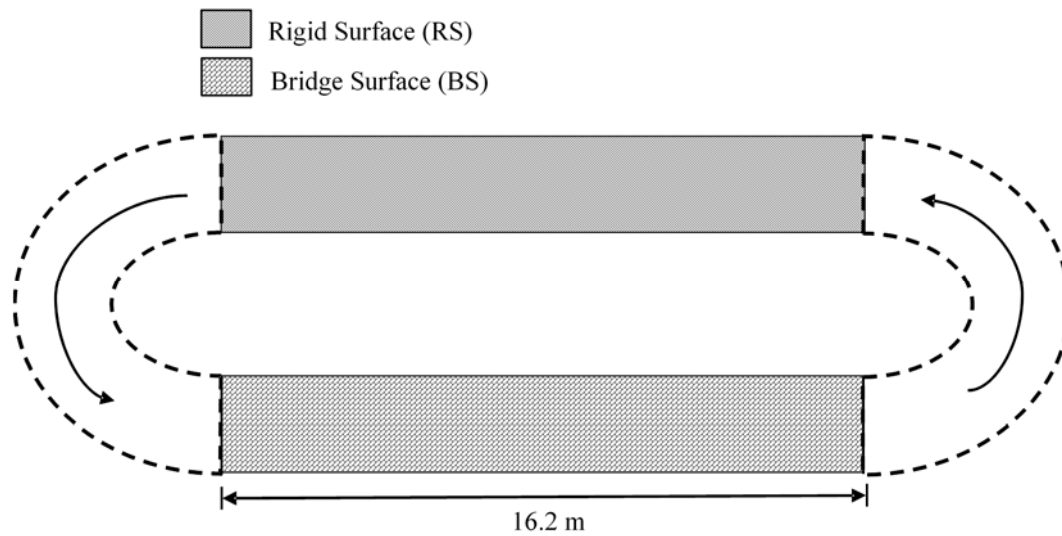
183 The tests comprised of walking at 2.4 Hz to excite the resonance by the first forcing harmonic,
184 walking at 1.2 Hz to excite the resonance by the second harmonic, and walking at 2.1 Hz to
185 expose the test subject to the beating vibration response. 2.4 Hz covers upper bound of normal
186 pacing frequency range of a pedestrian (1.6-2.4 Hz). In this paper, the pacing-to-bridge
187 frequency ratio ($\beta = f_p/f_b$) is used, and so $\beta \in \{0.5, 0.87, 1.0\}$.

188

189 Five test subjects (4 male, 1 female), weighing from 543 N to 1117 N participated in the
190 experiments. The test subject-to-bridge mass ratio, $\mu_m = m_p/m_b$ ranged from 0.33-0.7% and it
191 will be used later to discuss the results for each test subject. For each trial, test subjects walked
192 a circuit including a rigid surface (RS) and bridge surface (BS) as shown in Figure 4. On both
193 surfaces, the walking length was the same (16.2 m). After a sound signal, test subjects started
194 walking. A metronome was used during each trial so that test subjects targeted the desired
195 pacing frequency. Each walking trial was repeated until five successful trials were recorded. It
196 should be stated that all trials were carried out in accordance with The Code of Ethics of the
197 World Medical Association (Declaration of Helsinki).

198

199



200

201

202

Figure 4 Schematic plan of the walking trials path.

203 2.3 Data acquisition

204

205

206

207

208

209

210

211

212

213

214

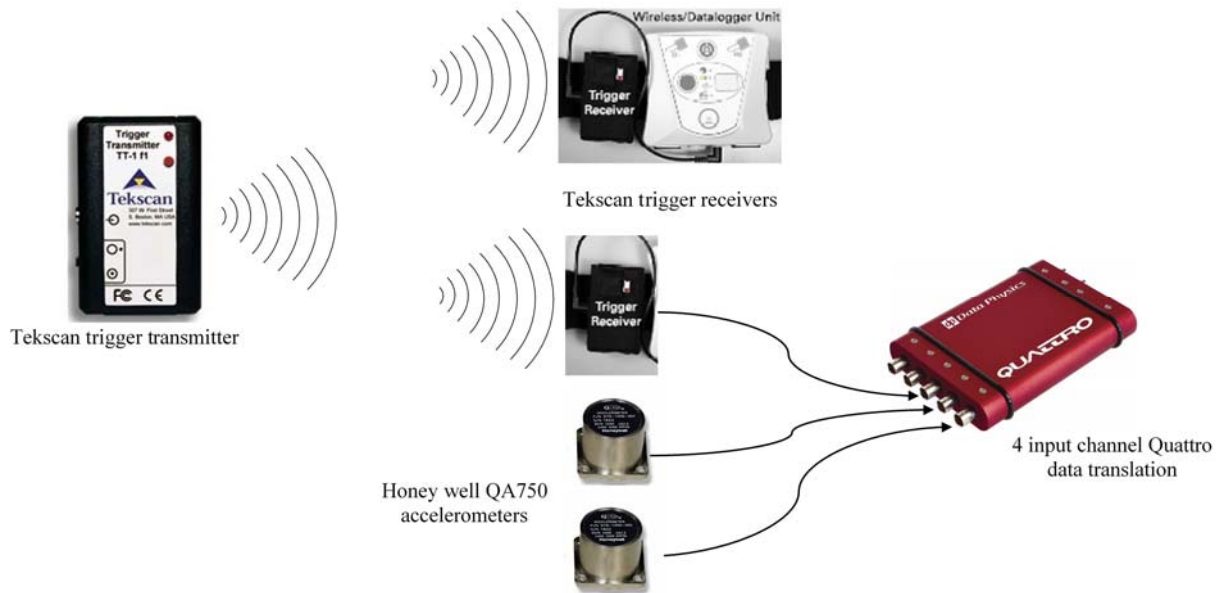
215

216

To record input forces and output accelerations data, a test set-up was designed as shown in Figure 5. The bridge vibration was measured using two Honeywell QA750 accelerometers, placed at mid-span and quarter-span points. The accelerometer signals were recorded using Quattro data acquisition (DAQ) unit by Data Physics (see Figure 5). The TekScan equipment was used for collecting the GRFs of the rigid and bridge surfaces throughout the walking trials. A TekScan trigger transmitter and two TekScan trigger receivers were used to synchronize recordings remotely. One trigger receiver was connected to the data recorder of the TekScan system, and the other one was attached to the Quattro DAQ. Note that unusually, the trigger was not used to trigger recording, rather its voltage output was recorded to identify the time window when the test subject was occupying the bridge. Thus, when the test subject was visually observed to be at the end of the footbridge a further trigger signal was given, changing the trigger output voltage, though data continued to be collected (e.g. free-vibration). Figure 6 shows a typical trigger voltage signal for the test subject of $\mu_m = 0.6\%$ and trial No. 5 with

217 frequency ratio of 1. This specific test subject, trial, and frequency ratio will be used as a
 218 running example through the paper.

219

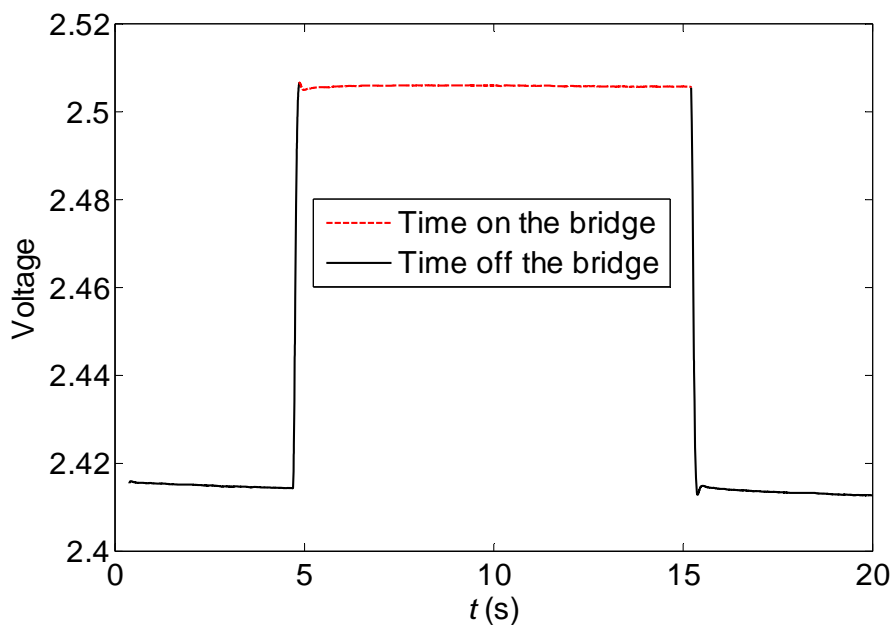


220

221

222

Figure 5 Test set-up for data acquisition.



223

224

225

226

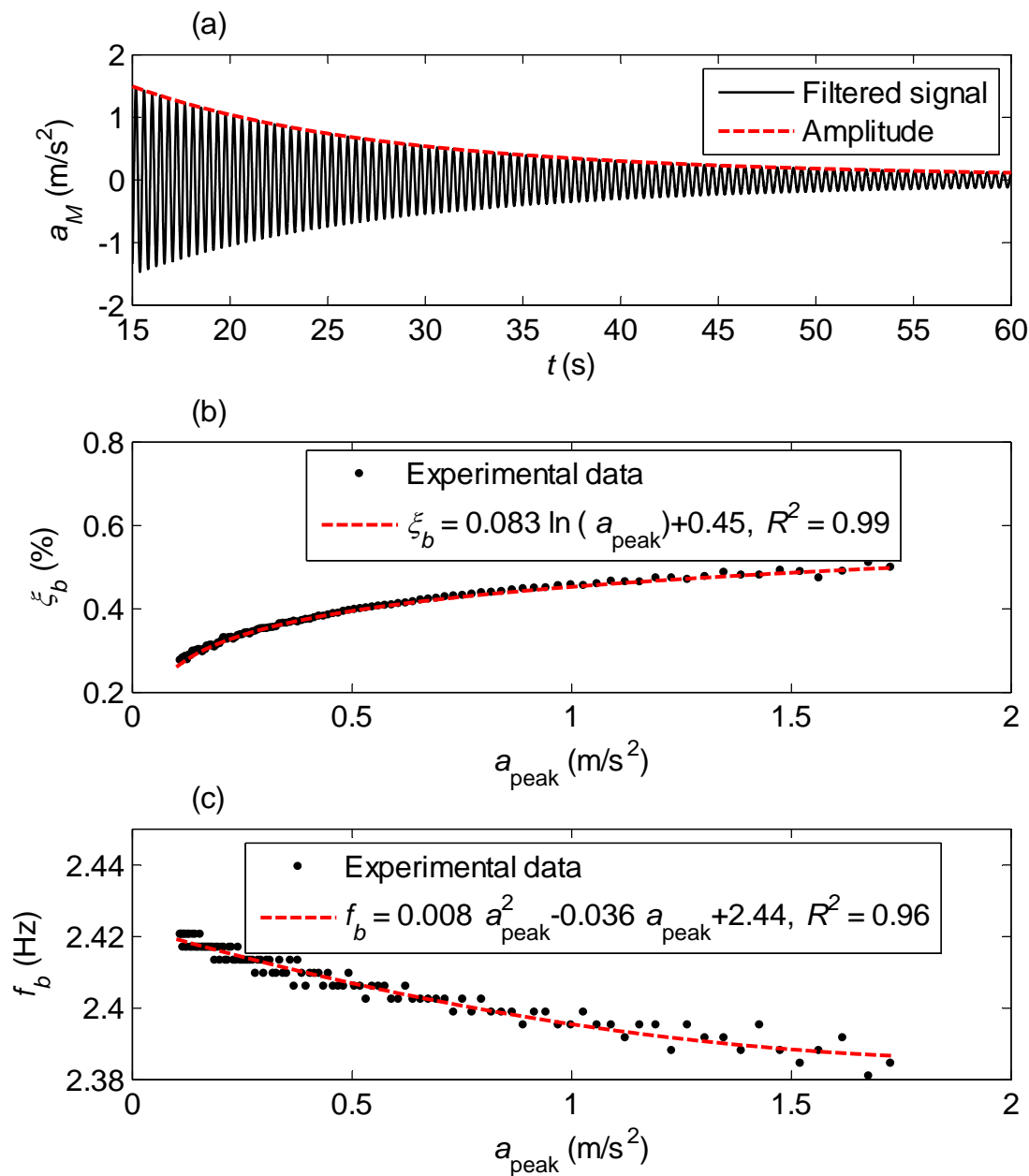
Figure 6 Voltage signal for time on and off the bridge for the example test subject, $\mu_m = 0.6\%$ and trial No. 5 with frequency ratio of 1.

227 **3. Experimental Results**

228 **3.1 Footbridge frequency and damping**

229 Free decay vibration measurements were made to investigate dynamic characteristics of the
230 footbridge. It was found that the bridge frequency, f_b , and damping, ζ_b , are amplitude-dependent.
231 To determine the bridge damping, an exponential decay curve is fitted (using least-squares) to
232 a moving window of five peaks (Figure 7a). It was found that the damping ratio increases with
233 an increase in the vibration amplitude, a_p , as shown in Figure 7b. This is a common feature of
234 real structures because there are more sources and increased energy dissipation at higher
235 vibration amplitudes. Nevertheless, the maximum damping ratio of about 0.5% is still quite
236 low, ensuring lively behaviour. The natural frequency was found to decrease slightly with an
237 increase in the vibration amplitude (Figure 7c). This is also typical behaviour in civil
238 engineering structures. Finally, data points were fitted to model the relationship between
239 damping and vibration amplitude, as well as frequency and vibration amplitude (Figures 7b
240 and 7c). These relationships are used in the numerical simulations.

241

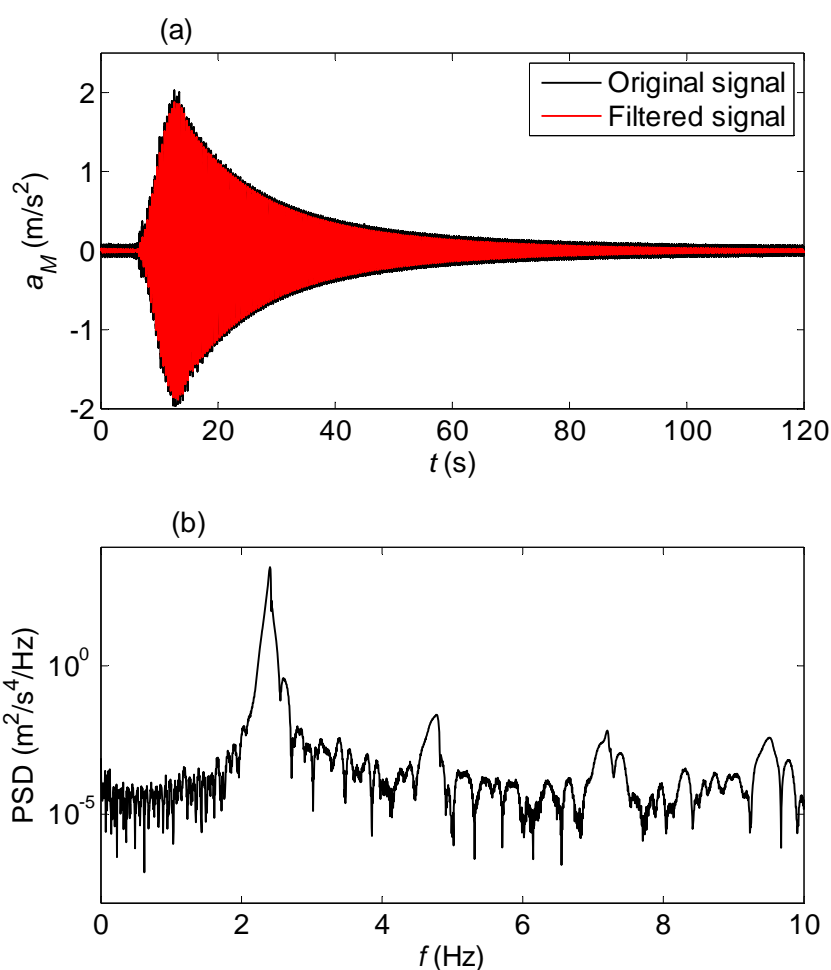


242 Figure 7 (a) free decay vibration time history and its amplitude for the bridge (a low-pass 4th order Butterworth
 243 filter with cut-off frequency, 10 Hz, was used); (b) amplitude-dependent bridge damping results and model (c)
 244 amplitude-dependent bridge frequency results and model.
 245
 246

247 3.2 Measured vibration responses

248 The mid-span acceleration response of the bridge to a walking trial, in which a test subject
 249 walked at 2.4 Hz (hereafter referred to as the exemplary test subject and trial), is illustrated in
 250 Figure 8a. Noise in the measured signal was removed using a low-pass 4th order Butterworth

251 filter with cut-off frequency of 10 Hz. The cut-off frequency of 10 Hz is more than four times
252 the bridge fundamental frequency and so the results will not be influenced by the filter roll-off.
253 The corresponding power spectrum density (PSD) of the acceleration signal, shown in Figure
254 8b, reveals that most of the response energy is concentrated at the first vibration mode of the
255 bridge.
256



257 Figure 8 (a) bridge mid-span acceleration response (b) its corresponding power spectral density (PSD) for the
258 exemplary test subject (trial of Figure 6).
259
260

261 The maximum response for each acceleration signal is selected as the response metric. Table 1
262 summarizes the maximum acceleration response, a_{max} , for each test subject, pacing frequency,
263 and trial. The maximum accelerations from Table 1 can be compared with the limits in the

264 Setra guideline [37], shown in Table 2. In many cases, the footbridge provides either “minimum”
 265 or “unacceptable vibration” comfort level to the test subject, demonstrating the liveliness of
 266 the structure.

267

268 Table 1. Maximum measured acceleration response (a_{max} , m/s²).

Test Subject	Mass Ratio, μ_m (%)	Frequency Ratio, β	Trial No.					Mean
			1	2	3	4	5	
1	0.33	0.50	0.22	0.22	0.21	0.22	0.25	0.22
		0.87	0.17	0.21	0.20	0.15	0.19	0.18
		1.00	1.32	1.40	1.28	1.24	1.33	1.31
2	0.40	0.50	0.19	0.17	0.17	0.18	0.20	0.18
		0.87	0.19	0.24	0.17	0.16	0.20	0.19
		1.00	1.26	1.43	1.32	1.28	1.26	1.31
3	0.50	0.50	0.16	0.25	0.15	0.20	0.18	0.19
		0.87	0.35	0.20	0.22	0.22	0.22	0.24
		1.00	1.33	1.05	1.43	1.32	1.43	1.31
4	0.60	0.50	0.25	0.23	0.25	0.37	0.30	0.28
		0.87	0.21	0.28	0.28	0.27	0.24	0.26
		1.00	1.34	1.83	1.82	1.84	1.87	1.74
5	0.70	0.50	0.49	0.53	0.46	0.62	0.57	0.53
		0.87	0.29	0.35	0.54	0.28	0.37	0.37
		1.00	2.48	2.38	2.63	2.50	2.53	2.51

269

270 Table 2. Comfort levels and acceleration ranges (from [7]).

Comfort Level	Degree of comfort	Vertical acceleration limits (m/s ²)
CL 1	Maximum	< 0.5
CL 2	Medium	0.5 – 1.0
CL 3	Minimum	1.0 – 2.5
CL 4	Unacceptable vibration	> 2.5

271

272 3.3 GRFs signal acquisition and processing

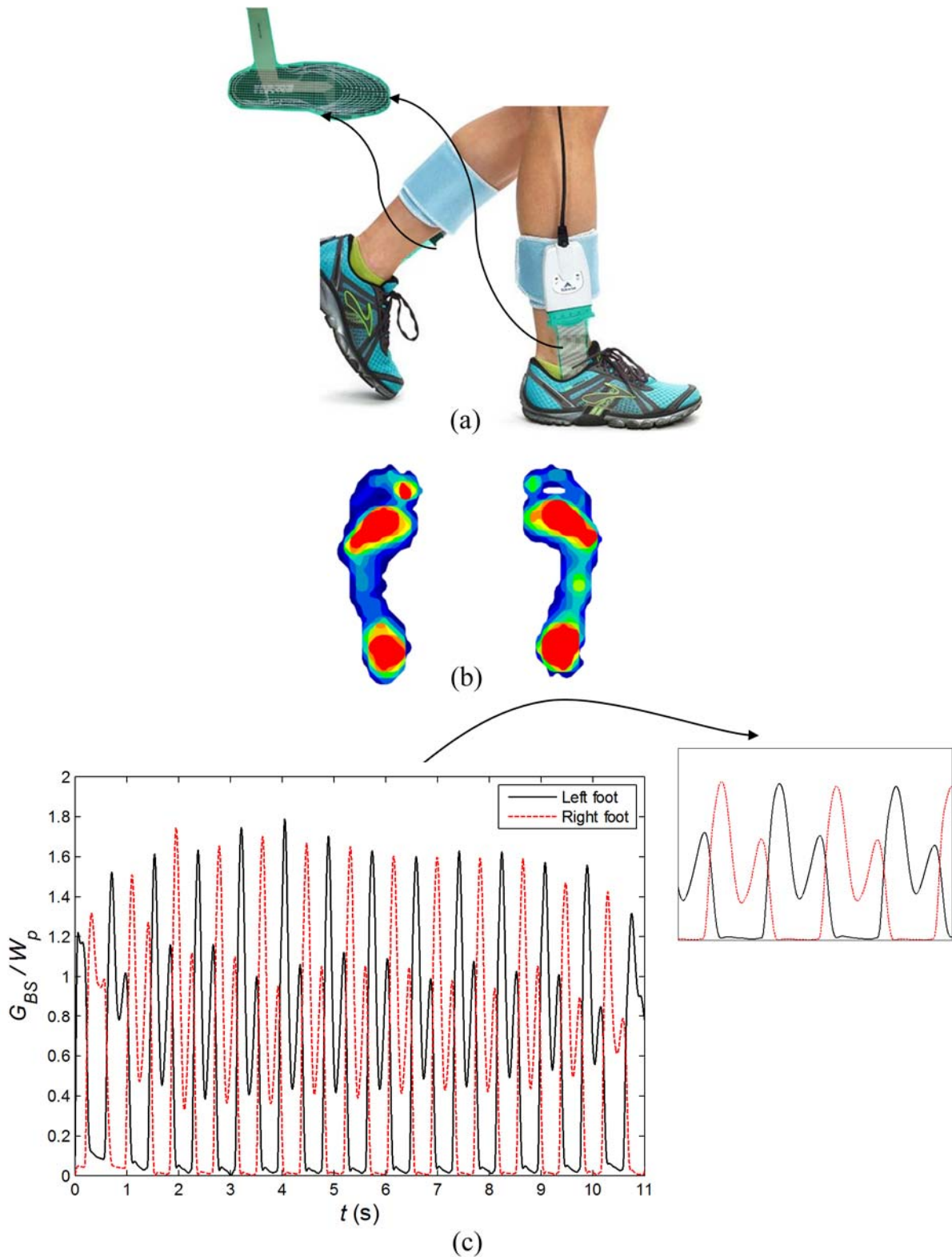
273 To measure the GRFs on both the rigid and flexible surfaces during walking, a novel
 274 experimental approach was employed. TekScan F-Scan in-shoe plantar pressure sensors
 275 developed for medical applications were used [3], [40], [41]. The measured pressure profiles

276 were integrated to determine force time histories for each foot allowing detailed gait analysis.
277 TekScan F-scan in-shoe sensors, pressure distribution, and bridge surface force signals, G_{BS} ,
278 of left and right feet for the exemplary test subject are shown in Figure 9.

279

280 The sensors are made up of 960 individual pressure sensing capacitor cells, which are referred
281 to as sensels. The sensels are arranged in rows and columns on each sensor. The 8-bit output
282 of each sensel is divided into $2^8 = 256$ increments, and displayed as a value (Raw Sum), in the
283 range of 0 to 255 by the F-scan software. If all sensels reach a raw count of 255, the
284 corresponding pressure is called saturation pressure. Although raw sum display shows relative
285 force differences on the sensor, this data is more meaningful if the force is calibrated to give
286 engineering measurement units. Obviously, proper calibration of the sensors is critical to
287 obtaining accurate force readings. When a test subject walks, there must be sufficient raw
288 output generated from the sensor so the calibration is accurate. It is also necessary to zero the
289 sensor output. Indeed, when one foot is supporting the body weight during walking, the other
290 foot is up in the air and its force should be zero. However, because the foot sensors are pre-
291 tensioned to the sole of the foot by shoe-lacing, the output of sensors is not zero when foot is
292 not touching the ground (Figure 9). Hence, it is necessary to zero the force output for each trial
293 during a swing phase of walking.

294

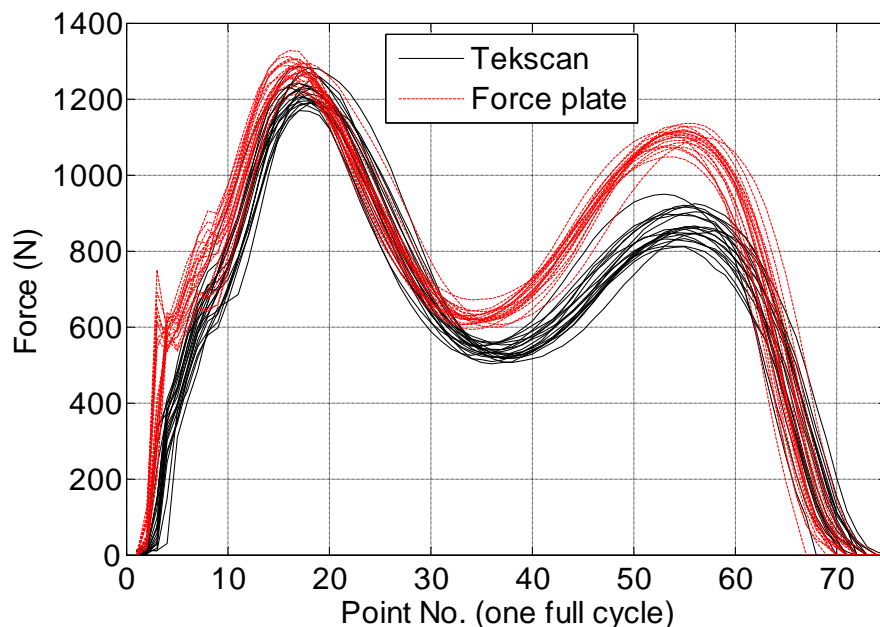


295
296 Figure 9 TekScan F-scan in-shoe sensors: (a) as worn by subject (image taken from [42] and used with permission
297 of Tekscan company), (b) output pressure distribution under a standing subject, and (c) bridge surface force signals
298 of left and right feet for the exemplary test subject.
299

300 The TekScan software supports five methods for calibrating sensors: point calibration, step
301 calibration, walk calibration, frame calibration, and two-point calibration. All of these methods

302 were considered for accuracy using a force plate as a benchmark before the main trials were
303 conducted. A walk calibration was found to give higher accuracy in the regions of interest
304 compared to step calibration using the same factors. Of most interest, step calibration and walk
305 calibration use the test subject's weight to adjust the calibration factor. As seen in Figure 10,
306 the walk calibration estimates walking force with an accuracy considered reasonable for this
307 work. It gives good result for the heel-strike phase while it underestimates the pedestrian force
308 somewhat for toe-off phase. Calibration of the sensor is carried out for each trial using the test
309 subject weight and rigid surface force time history. Thus, each trial conducted has its own
310 calibration factor.

311

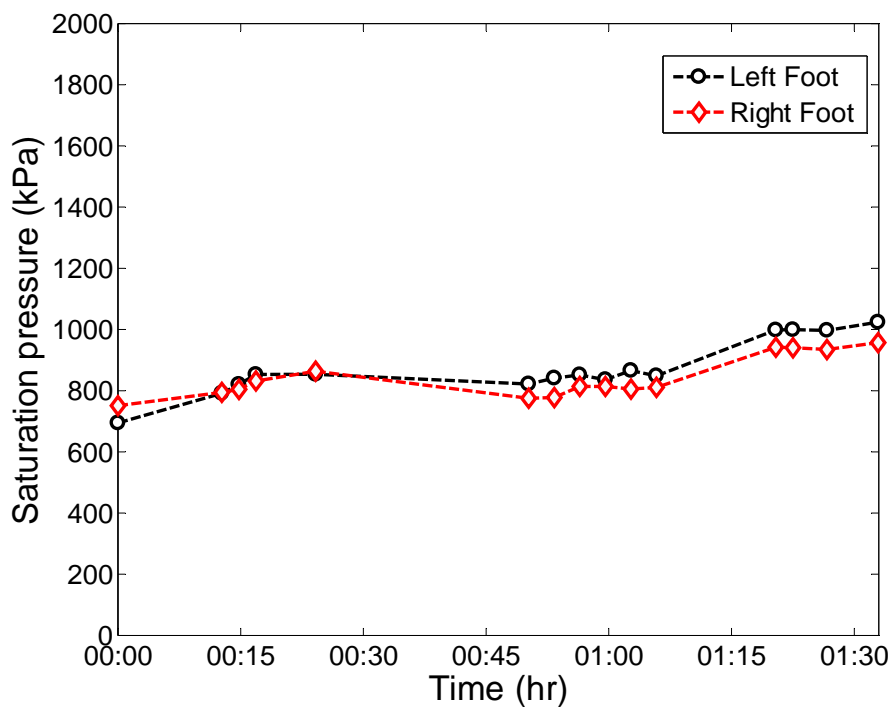


312 Figure 10 TekScan (walk calibration) and force plate results for pacing frequency of 2 Hz, 20 trials, left foot,
313 and one full cycle.
314

315

316 There is one further aspect of the TekScan sensors that benefits from giving each trial its own
317 calibration factor. Due to degradation of the sensor, drift of the sensor output can occur over
318 time. Additionally, the sensors can deteriorate so that rows or columns of the sensels no longer
319 export forces. Saturation pressure (described above) is closely related to the calibration factor.

320 Therefore, if some sensors damage during walking, the saturation pressure will change and so
 321 this was tracked throughout the trials. Figure 11 shows a sample of saturation pressure record
 322 for one test subject for the pacing frequency of 2.4 Hz. It can be seen that sensor degradation
 323 is small because the saturation pressures over a period of about 1.5 hours remain reasonably
 324 consistent.



325 Figure 11 Saturation pressure vs. time (hour) for one test subject and pacing frequency of 2.4 Hz.
 326
 327

325
 326
 327

328 4. Data Analysis

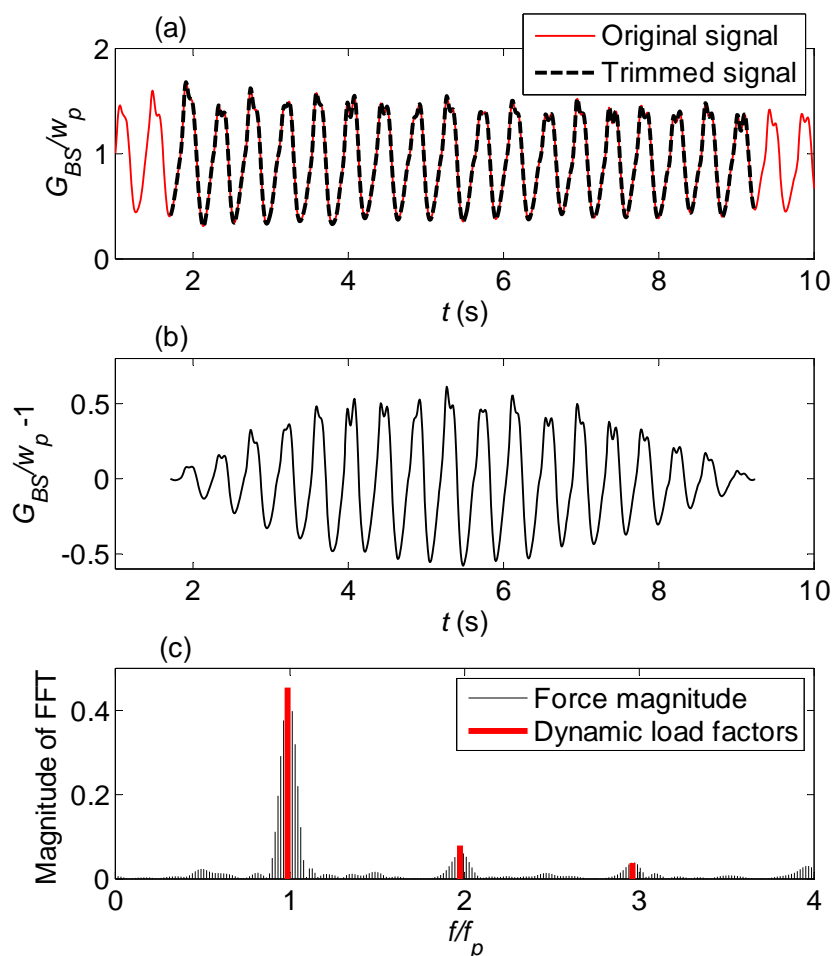
329 4.1 Dynamic load factors

330 Walking forces are commonly described using a Fourier series [24]:

$$331 \quad G(t) = W_p \sum_{k=0}^r \text{DLF}_k \cos(2\pi k f_p t + \varphi_k) \quad (1)$$

332 where $W_p = m_p g$; m_p is the pedestrian mass; g is the acceleration due to gravity; f_p is the pacing
 333 frequency; and DLF_k is the dynamic load factor for the k th harmonic. The phase angle of the
 334 k th harmonic is denoted by φ_k , and r represents total number of harmonics considered. In this

335 representation, the harmonic $k = 0$ corresponds to the static pedestrian weight, and so $\varphi_0 = 0$ to
336 give $DLF_0 = 1$. To calculate the DLFs from the GRF measurements, the start and end of the
337 recorded walking force signals are trimmed such that a signal consists of some even number of
338 full steps achieved. Then, the DC component is subtracted from the signal and then the signal
339 is windowed using a Hann window to suppress leakage. The signal is zero-padded afterwards
340 and transformed into the frequency domain using the Fast Fourier Transform (FFT). The signal
341 amplitude in the frequency domain is corrected for the side-lobe loss due to using Hann window
342 [43]. Figure 12 shows all steps to determine dynamic load factor for the exemplary test subject,
343 highlighting the first four DLFs. Consistent with the literature, the pedestrian force is not
344 perfectly periodic; in fact, it is a narrow band signal with some of its energy spread to adjacent
345 frequencies [44], [45]. Phase angles are also found to be more or less uniformly distributed
346 from 0 to π radians.
347



348 Figure 12 Determination of walking DLFs: (a) Tekscan original and trimmed force signal (b) windowed
 349 trimmed signal (b) Fast Fourier Transform of the trimmed signal with frequency resolution, 0.01 Hz (the
 350 variability in FFT might not be representative of normal walking due to setting the pacing frequency with the
 351 metronome, and some of the energy spread to adjacent frequencies is due to leakage from the use of the Hann
 352 window).
 353
 354

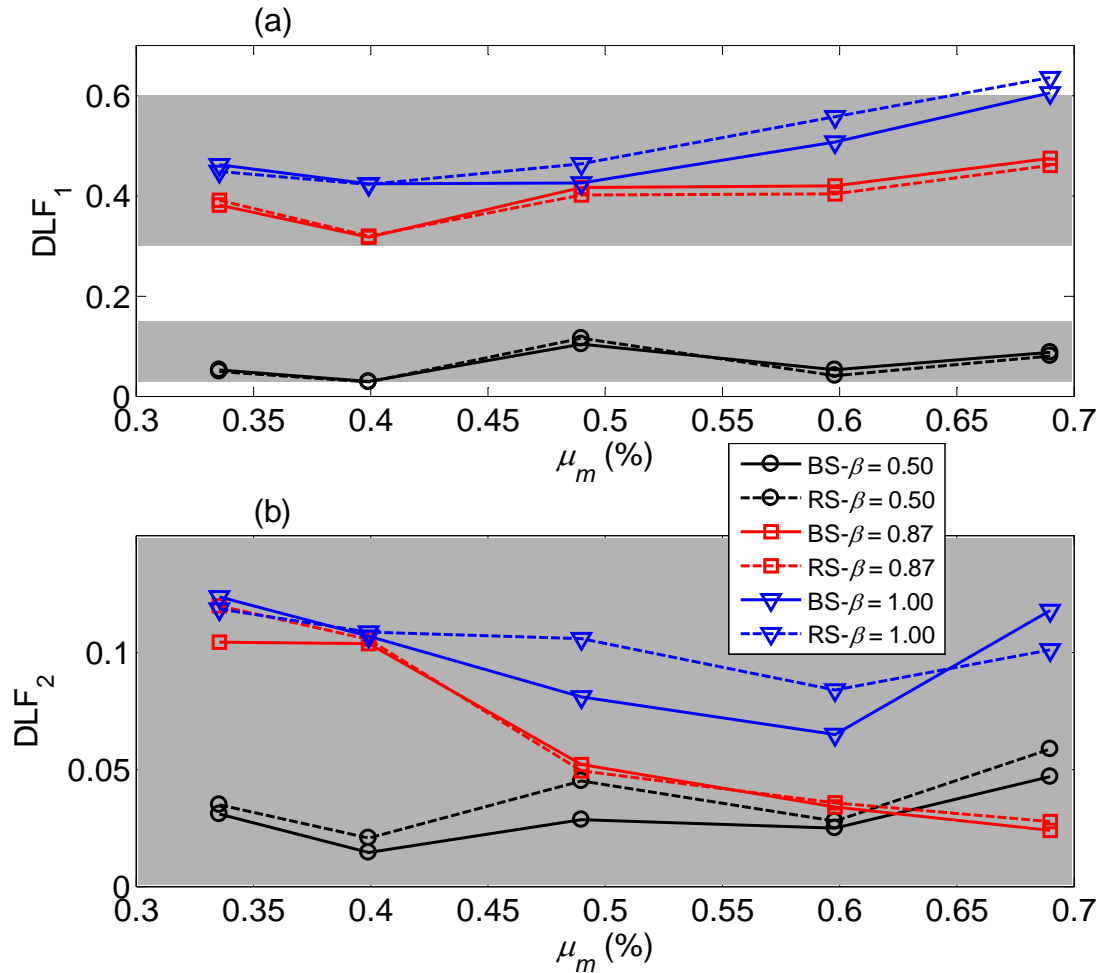
355 For each trial and surface (rigid and bridge surface), first two DLFs of pedestrian force are
 356 calculated. Then, the mean DLF is taken across the five trials for each test subject for a specific
 357 pacing frequency. Figure 13 illustrates the mean first and second DLF for different frequency
 358 ratios and mass ratios (the grey regions show Kerr's DLFs [46]). As seen in Figure 13a, for the
 359 resonance case, $\beta = 1$, the difference between the mean first DLF of the rigid and bridge
 360 surfaces is significant. As the mass ratio increases, this difference tends to increase. However,
 361 the difference is not monotonically increasing. From Figure 13b, it is clear that, for resonances
 362 by both first and second harmonic, $\beta = 1$ and $\beta = 0.5$, there is a substantial difference between

363 second mean DLFs of rigid and bridge surface. Furthermore, the DLFs on the bridge surface
364 are smaller than those on the rigid surface for $\beta = 1$. When β becomes far from 1 (i.e. $\beta = 0.87$,
365 0.5), the difference in first DLFs gets smaller, and it seems that the vibrating bridge does not
366 have a significant effect on the mean DLFs. The second DLFs of the bridge surface are smaller
367 than those of the rigid surface for both resonance and second harmonic excitation, $\beta = 1$ and β
368 = 0.5. Considering then the postulated S2HI effect, the bridge surface DLFs can be expressed
369 as:

$$370 \quad DLF_{BS} = DLF_{RS} - \Delta DLF_{S2HI} \quad (2)$$

371 which DLF_{BS} and DLF_{RS} are dynamic load factors of human force on bridge and rigid
372 surfaces, respectively; ΔDLF_{S2HI} is the change in the dynamic force due to the S2HI effects
373 caused by the vibration. It should be mentioned that as the test subject gets heavier, this effect
374 typically becomes more pronounced.

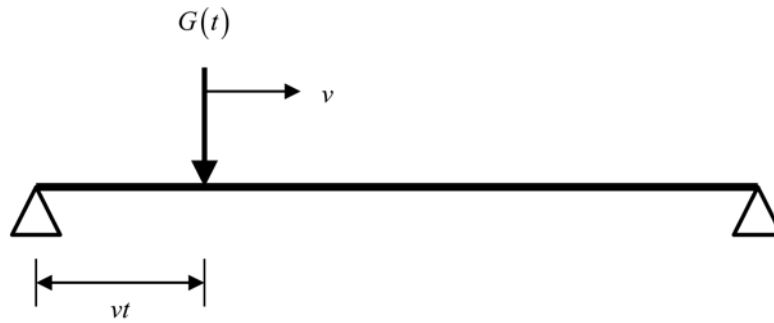
375
376 The drop in DLF_1 on the lively surface was also found in [47], [23] in which it was explained
377 as being a consequence of a vibration-induced ‘self-excited force’. This concept suggests that
378 there are two components combine to give the GRF on the bridge surface, G_{BS} : rigid surface
379 force, G_{RS} and S2HI force component, G_{S2HI} . However, there is not yet an accepted definition
380 of what amount of HSI is to be characterized as “self-excited”.



381 Figure 13 Mean dynamic load factor of (a) first harmonic (b) second harmonic versus mass ratio for different
 382 frequency ratios, showing Kerr's [46] DLF regions (greyed) (RS and BS stand for rigid surface and bridge
 383 surface respectively).
 384

386 4.2 Simulated and measured vibration response

387 The analytical model used to simulate vibration response is shown in Figure 14. The pedestrian
 388 is modelled as a force moving at constant velocity and the bridge is modelled as a simply-
 389 supported beam in modal space considering only the first mode of the vibration. The measured
 390 force, $G(t)$, moving at the actual average velocity as recorded in each trial is used in simulations.
 391 As previously mentioned, the bridge frequency and damping are amplitude-dependent, and this
 392 is considered in the numerical model.



394
395

Figure 14 Analytical modelling of human-bridge system.

396

397 The equation of motion in modal space is [24]:

398
$$\ddot{q}(t) + 2\xi_b \omega_b \dot{q}(t) + \omega_b^2 q(t) = \frac{\phi(x) G(t)}{M_b} \delta(x - vt) \quad (3)$$

399 where q , \dot{q} and \ddot{q} are the modal displacement, velocity, and acceleration for the first mode of

400 the bridge; ξ_b and ω_b are the vibration amplitude-dependent damping and circular frequency

401 of the first mode; they are updated for each amplitude of vibration [48]; M_b and $\phi(x)$ are the

402 modal mass and mode shape; $G(t)$ is the measured human force on either rigid or bridge

403 surface (G_{RS} or G_{BS}); δ is Dirac delta function; x is a position on the bridge; and vt is the

404 pedestrian location at time t , while v is the average velocity of the traverse. The modal vibration

405 response of the bridge is obtained using Newmark- β integration. Finally, vibration response of

406 the bridge in physical coordinates at any location is given by:

407
$$w(x, t) = \phi(x) q(t) \quad (4)$$

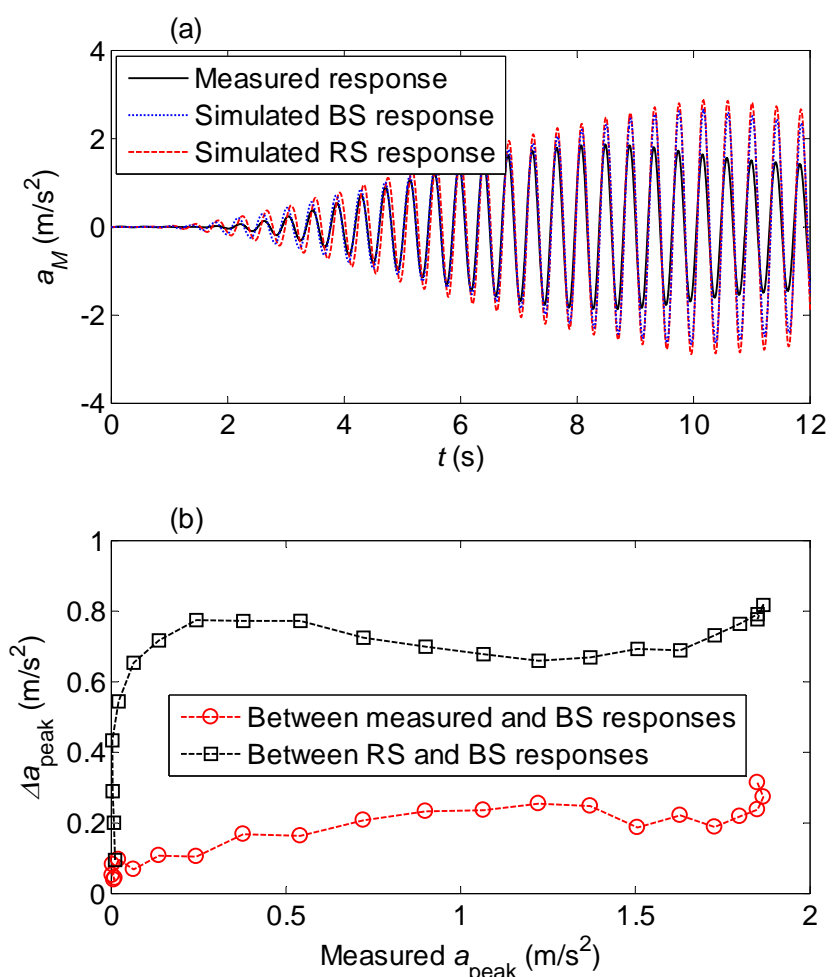
408 where the mode shape can be approximated by a half-sine function [49]:

409
$$\phi(x) = \sin\left(\frac{\pi x}{L}\right) \quad (5)$$

410 where L is the bridge length. Figure 15a shows the measured vibration response and simulated

411 RS, and BS responses at the bridge mid-span for the exemplary test subject. The measured

412 accelerations are seen to be smaller than that simulated by the numerical model, even when
 413 using the measured induced force to the bridge surface. The difference between the peak
 414 amplitudes of measured and both forms of simulated vibrations for the exemplary test subject
 415 are shown in Figure 15b. The differences between the RS and BS responses as well as between
 416 the measured and BS responses become more and more obvious as the response amplitude
 417 increases. However, these differences have sporadic increasing and decreasing trends. Further,
 418 in this example, the difference is far more significant between measured and BS responses,
 419 than between RS and BS responses.



420 Figure 15 (a) Measured response (from the experiment), simulated BS, and RS responses (from the numerical
 421 model) (b) differences between peak amplitudes of the responses of (a) – see Figure 2 for meaning.
 422
 423

424 The maximum of each acceleration time history, a_{max} , is used as a response metric. Maximum
 425 root-mean-square (RMS) could be used instead, but is directly proportional to the peak

426 acceleration over a few cycles of vibration, and so response ratios are unaffected by the measure
 427 used. The results are given in Tables 3 (RS responses) and 4 (BS responses), and shown in
 428 Figure 16. The variability of results is low with coefficient of variation up to 0.29 and central
 429 tendencies are therefore meaningful to describe the results.

430

431 Table 3. Maximum acceleration response (a_{max} , m/s²) of the numerical model using the measured rigid surface
 432 GRFs.

Test Subject	Mass Ratio, μ_m (%)	Frequency Ratio, β	Trial No.					Mean
			1	2	3	4	5	
1	0.33	0.50	0.10	0.24	0.18	0.16	0.18	0.17
		0.87	0.17	0.19	0.24	0.15	0.19	0.19
		1.00	1.13	1.34	1.29	1.53	1.45	1.35
2	0.40	0.50	0.14	0.13	0.16	0.16	0.11	0.14
		0.87	0.17	0.18	0.21	0.15	0.15	0.17
		1.00	1.38	1.31	1.49	1.52	1.52	1.44
3	0.50	0.50	0.14	0.14	0.14	0.16	0.15	0.15
		0.87	0.34	0.23	0.31	0.33	0.23	0.29
		1.00	2.06	2.02	1.97	1.79	1.68	1.90
4	0.60	0.50	0.27	0.29	0.25	0.22	0.26	0.26
		0.87	0.33	0.31	0.29	0.31	0.32	0.31
		1.00	2.98	2.28	3.11	2.95	2.96	2.86
5	0.70	0.50	0.63	0.56	0.65	0.53	0.42	0.56
		0.87	0.36	0.38	0.42	0.34	0.42	0.38
		1.00	2.19	3.36	1.62	3.48	2.91	2.71

433

434 Table 4. Maximum acceleration response (a_{max} , m/s²) of the numerical model using the measured bridge surface
 435 GRFs.

Test Subject	Mass Ratio, μ_m (%)	Frequency Ratio, β	Trial No.					Mean
			1	2	3	4	5	
1	0.33	0.50	0.22	0.23	0.12	0.24	0.21	0.20
		0.87	0.17	0.25	0.22	0.19	0.18	0.20
		1.00	1.31	1.42	1.31	1.38	1.34	1.35
2	0.40	0.50	0.09	0.06	0.09	0.07	0.06	0.07
		0.87	0.17	0.19	0.16	0.14	0.08	0.15
		1.00	1.10	1.53	1.46	1.37	1.27	1.35
3	0.50	0.50	0.17	0.21	0.12	0.11	0.15	0.15

		0.87	0.37	0.26	0.30	0.26	0.24	0.28
		1.00	1.65	1.07	1.76	1.51	1.59	1.52
		0.50	0.23	0.20	0.19	0.30	0.27	0.24
4	0.60	0.87	0.27	0.29	0.25	0.22	0.26	0.26
		1.00	1.54	1.86	2.42	2.27	2.68	2.15
		0.50	0.47	0.49	0.47	0.59	0.65	0.53
5	0.70	0.87	0.29	0.40	0.44	0.32	0.39	0.37
		1.00	3.22	3.29	3.62	3.26	3.26	3.33

436

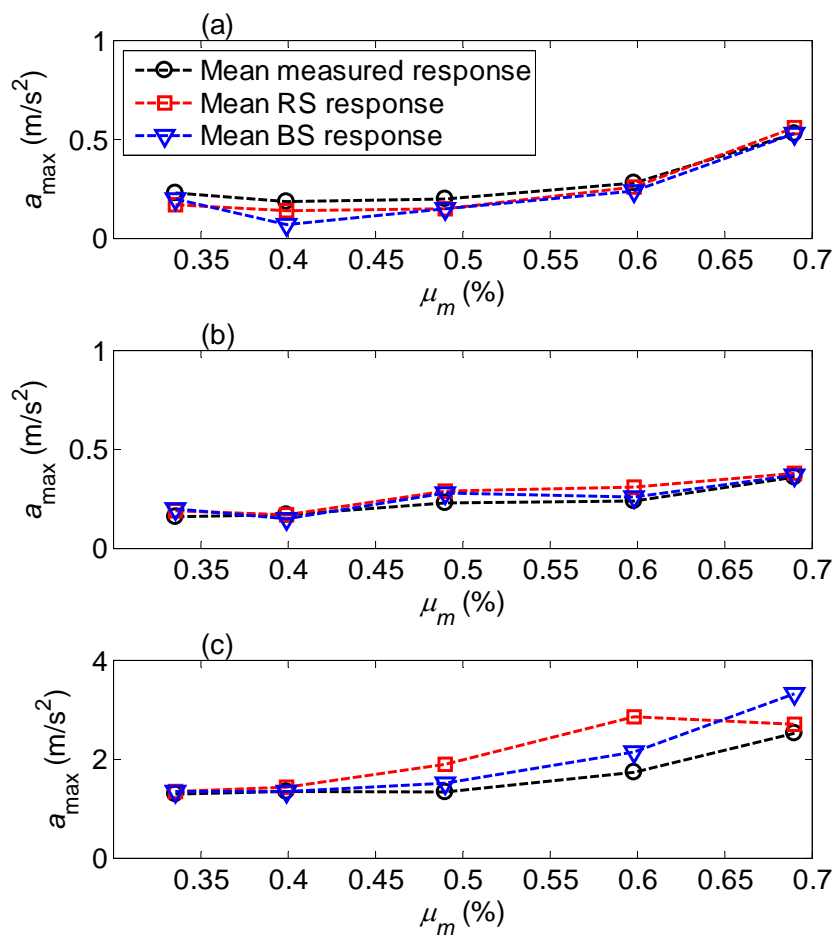
437 To perform further analysis and understand the central tendency of the simulated and measured
 438 responses, an average is taken across trials for each test subject with a specific pacing frequency,
 439 and it is shown in the last column of Tables 3 and 4. For $\beta = 1$ the RS response is greater than
 440 the BS response for almost all test subjects except for the test subject with mass ratio 0.70%.
 441 The BS response is significantly larger than the measured response for all cases at frequency
 442 ratio of 1. As shown in the experimental-numerical programme (Figure 2), these differences
 443 between RS and BS responses, and between BS and measured responses reflect S2HI and H2SI,
 444 respectively. Hence, excluding S2HI and H2SI overestimates vibration response by up to 32%
 445 and 33%, respectively (see Figure 16c).

446

447 The overestimation of vibration response as a result of ignoring both HSI forms may lead to
 448 vibration serviceability assessment failure of a bridge, while it may in truth be serviceable.
 449 Both S2HI and H2SI effects increase as frequency ratio and mass ratio increase (Figure 16c).
 450 For S2HI, it means that its influence on the walking force acting on the bridge surface increases,
 451 both as the vibration amplitude tends to increase and as the test subject gets heavier. For H2SI,
 452 the effects of the test subjects' mass and pacing frequency support the hypothesis that the
 453 human body can act as a dynamic absorber. When the pacing frequency of the test subject
 454 (absorber frequency) is close to the bridge frequency, the energy dissipated by the pedestrian

455 increases. Also, as the test subject (absorber) gets heavier, it seems that more energy is damped
 456 out of the bridge.

457



458 Figure 16 Mean maximum acceleration for frequency ratio of: (a) 0.50 (b) 0.87 (c) 1. See Figure 2 to understand
 459 why the blue (BS) to black (measured) lines reflects the effect of H2SI and red (RS) to blue, that of S2HI.
 460
 461

462 5. Statistical Tests

463 In section 4.2, it was shown that the differences between mean responses are large at resonance.
 464 These differences are an indication of HSI as per Figure 2. However, two important caveats
 465 must be considered regarding the results. First, a small number of five trials for each test subject
 466 and pacing frequency was used to calculate the mean maximum acceleration response for the
 467 simulated RS and BS vibration response and measured vibration response. The question then
 468 is, to what extent the small number of trials reflect the real (population) difference between

469 mean vibration responses. In other words, are the differences in means by chance or
470 representative of the population of responses as a whole? To answer this, parametric statistical
471 hypothesis testing is used. Second, careful consideration must be given to measurement
472 inaccuracies input to the numerical model which consequently influence the simulated
473 vibration responses. To quantify this, the input parameters are described in terms of probability
474 density functions (PDFs) and Monte Carlo simulations of output responses conducted. This
475 allows a broader understanding of the differences between the results, and hence the
476 quantitative influence of HSI in a probabilistic sense.

477

478 **5.1 Parametric test (hypothesis test)**

479 A parametric test makes assumptions about the underlying distribution of the population from
480 which the sample is being drawn. The population distribution of responses is assumed to be
481 normal, which can be reasonably justified through the central limit theorem [50]. According to
482 the experimental-numerical programme (Figure 2), the null, H_0 , and alternative hypotheses, H_1 ,
483 for each HSI form are given as:

484 1) S2HI:

$$485 \begin{cases} H_0 : \bar{R}_{RS} - \bar{R}_{BS} = 0 \\ H_1 : \bar{R}_{RS} - \bar{R}_{BS} \neq 0 \end{cases} \quad (6)$$

486 2) H2SI:

$$487 \begin{cases} H_0 : \bar{R}_{BS} - \bar{R}_M = 0 \\ H_1 : \bar{R}_{BS} - \bar{R}_M \neq 0 \end{cases} \quad (7)$$

488 where \bar{R}_{RS} , \bar{R}_{BS} , and \bar{R}_M stand for the mean response metric for the simulated RS, BS, and
489 measured cases respectively for a large population of trials. If null hypothesis, H_0 , is correct it
490 means that HSI is not significant, and that the difference in the means of two small samples are

491 by chance; otherwise, the alternative hypothesis, H_1 , is more likely and HSI exists in the
492 population of vibration responses.

493

494 When performing the hypothesis test, no HSI (null hypothesis) might be reached or two errors
495 could be made: incorrectly accepting HSI when it does not exist (error of the first kind) or
496 rejecting it when it does exist (error of the second kind). It is desirable to minimize the
497 probabilities of the two types of error. However, these errors cannot be controlled. Therefore,
498 a level of significance, α , is assigned to the probability of incorrectly accepting HSI when it
499 does not exist and then the error due to rejecting HSI when it does exist is minimized. The
500 standard way to remove the arbitrary choice of α is to report the p -value of the test, defined as
501 the smallest level of significance leading to accepting the alternative hypothesis (i.e. that HSI
502 exists). The p -value gives an idea of how strongly the data contradicts the hypothesis that there
503 is no HSI of any form. A small p -value shows that the mean response metrics are highly likely
504 to be different, and hence HSI exists.

505

506 To test the difference between the two samples for each form of HSI (see Figure 2 and
507 equations (6) and (7)), the two-sided independent sample Student's t -test is used, with equal
508 variances assumed for both populations. Table 5 summarizes the hypothesis test results for
509 both HSI forms for each pacing frequency, as assessed using the maximum acceleration
510 response metric (Tables 1, 3, and 4). It is clear that HSI only has significance for the $\beta = 1$ case
511 (for which p -values are small) while for the other frequency ratios, HSI mostly does not have
512 a statistically significant effect on the result. Considering then just the resonant case, for both
513 HSI forms, it can be seen that higher mass ratios mostly gives smaller p -values. This means
514 that the effect of HSI effect increases with mass ratio (as may be expected). However, typically
515 p -values resulting from H2SI, especially for heavy test subjects, are smaller than those of S2HI,

516 indicating that the effect of HSI on the dynamic properties of the system is more pronounced
 517 than the effect of the structure on the pedestrian walking force. There are some unexpected
 518 cases though for the mass ratios of 0.40% and 0.50%. Nevertheless, overall for the resonant
 519 case ($\beta = 1$), the results give strong support to the existence of H2SI, and somewhat weaker
 520 support to S2HI and show that the mass ratio is an important factor.

521

522 Table 5. p -values for the two postulated forms of HSI from the t -test for the maximum acceleration metric.

Test Subject	μ_m (%)	$\beta = 0.5$		$\beta = 0.87$		$\beta = 1$	
		S2HI	H2SI	S2HI	H2SI	S2HI	H2SI
1	0.33	0.33	0.40	0.52	0.35	0.96	0.29
2	0.40	0.41	0.54	0.30	0.10	0.29	0.67
3	0.50	0.75	0.19	0.95	0.25	0.02	0.17
4	0.60	0.43	0.24	0.72	0.92	0.05	0.02
5	0.70	0.67	1.00	0.63	0.97	0.13	0.00

523

524 **5.2 Non-parametric test (Monte Carlo Simulation)**

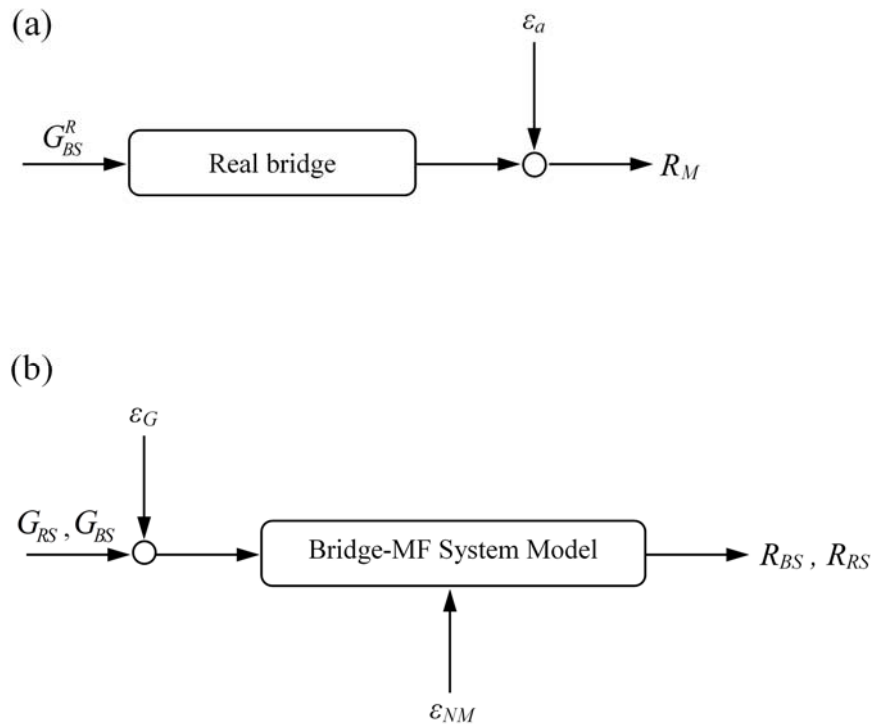
525 Non-parametric testing is used to determine the effects of measurement and model errors on
 526 the numerical model vibration response, and hence the conclusions drawn from these results.

527 Such errors could affect the HSI quantification, since the postulated HSI forms are defined in
 528 terms of differences between simulated and measured responses. Figure 17 illustrates a
 529 schematic view of potential errors in the experimental-numerical programme (also refer to
 530 Figure 2). It includes the real bridge, numerical model inputs and outputs, as well as errors.

531 The first type of error is measurement error. G_{BS}^R is the real (true) force without any error
 532 inputted into the real bridge. R_M is the measured response of the bridge with possible error, ε_a ,
 533 for one walking trial. This error is assumed negligible as the accelerometers used to measure
 534 the bridge response (Honeywell QA750) are of very high quality, with very low noise floor
 535 and output frequency response down to DC. The final measurement error is due to the GRF

536 measurement system, TekScan, denoted ε_G , which influences the measured pedestrian forces,
 537 G_{BS} and G_{RS} .

538



539
 540
 541

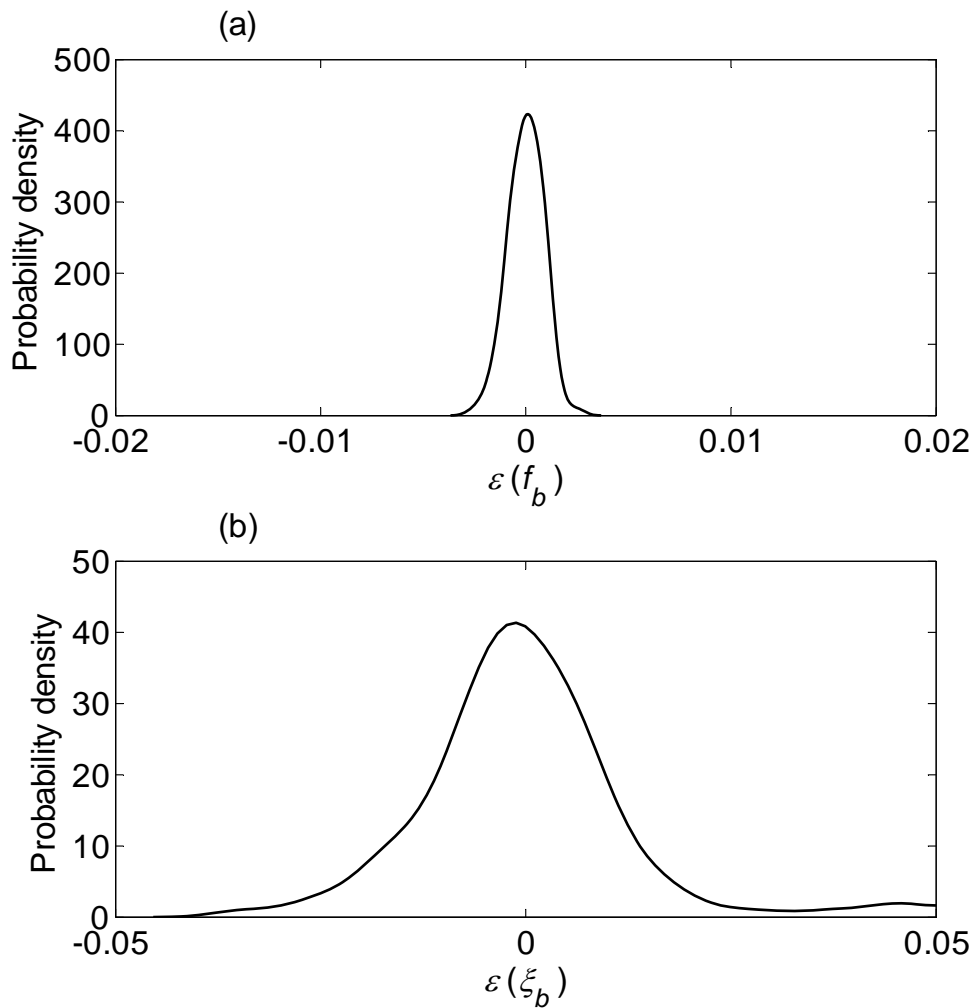
Figure 17 Schematic view of errors for: (a) real bridge (b) numerical model.

542 The second type of error is the error of the numerical model, ε_{NM} , which reflects the ability of
 543 the (simple) model to replicate reality. This error emanates from many possible sources which
 544 do occur but are not adequately captured in the model, such as the actual damping, frequency,
 545 mass, frictions/nonlinearities, nonlinear material behaviour, etc. In particular, the effects of the
 546 bridge damping and frequency are significant at resonance: small changes in these strongly
 547 affect the vibration response and so these are considered in detail. Each considered model
 548 parameter error is defined as:

549
$$\varepsilon(X) = \frac{X_{BM} - X}{X} \quad (8)$$

550 where X_{BM} is the benchmark value for the parameter, X . For the bridge damping and frequency,
 551 the free vibration results at the end of each trial were taken as the benchmark values, which is

552 reasonable since any ε_a is extremely small as noted above. Thus, the errors are estimated for
553 the bridge damping and frequency using equation (8). Kernel density estimation is then used
554 to estimate the PDF of the errors for each variable [51]. Figure 18 shows the PDFs of the errors
555 for bridge frequency and damping.



556 Figure 18 Probability density of bridge: (a) frequency (b) damping.
557
558

559 For the GRFs, the results of the force plate are treated as the benchmark or ‘true’ values. The
560 Tekscan system generally gives different force estimate. To model the true force from the
561 Tekscan measurements, the Tekscan error is analysed statistically. Since the sample rate is the
562 same for both the force plate and Tekscan, time is indicated by the index, i . Index j is used to

563 denote a specific trial of which there are N . The Tekscan measurement relative error for trial j
564 at time i is:

$$565 \quad \varepsilon_{ij} = \frac{G_{ij}^{FP} - G_{ij}^{TS}}{G_{ij}^{TS}} \quad (9)$$

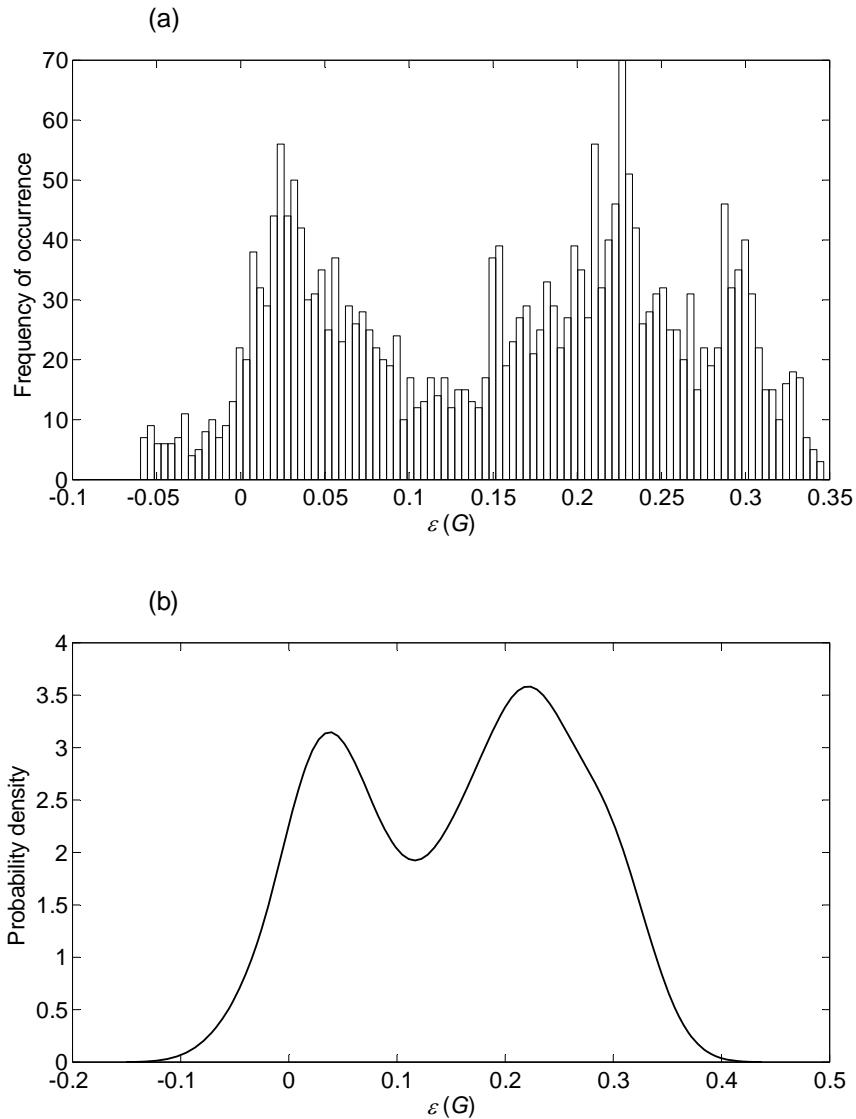
566 Figure 19a shows the histogram of ε_{ij} for all trials, and Figure 19b illustrates the probability
567 density of the relative errors using Kernel density estimation [51]. As a conservative estimation
568 of the Tekscan error, this probability density function is used to generate relative random errors,
569 ξ_i , which are employed to generate random representative force plate footsteps:

$$570 \quad G_i^{FP} = (1 + \xi_i) G_i^{TS} \quad (10)$$

571 Finally, randomly generated representative force plate footsteps are combined to create a
572 continuous force plate GRF.

573

574 Using this procedure for input force, and PDFs (Figure 18) for bridge frequency, and damping,
575 10^4 Monte Carlo simulations (MCSs) are performed to determine the variability of results due
576 to these possible errors. It is emphasized that the PDFs used are nonparametric (i.e. directly
577 those of Figures 18 and 19b), and so no additional error is introduced by assuming a parametric
578 PDF form (e.g. normal, lognormal).

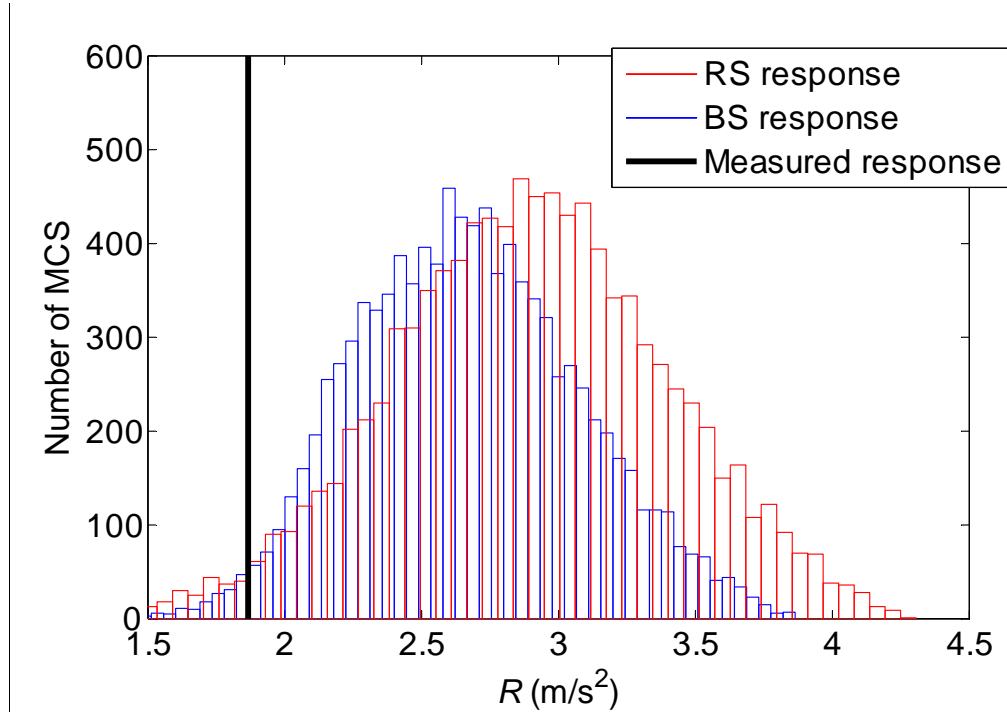


579
580 Figure 19. Tekscan measurement relative error: (a) histogram (b) probability density.
581

582 By way of example, Figure 20 shows the resulting histograms for possible RS and BS responses
583 considering the model errors, along with the actual corresponding measured response for the
584 exemplary test subject. The figure suggests that the RS and BS response distributions are
585 strongly biased with respect to the measurement. This is due to the very wide error distribution
586 taken for the Tekscan error; unfortunately no better error model is available. Nevertheless, in
587 a relative sense, there is a difference between the distributions for RS and BS forces. According
588 to the experimental-numerical framework of Figure 2, this then, is the influence of HSI.

589 Further, the distance between the mean and measurement reflects to some extent the error of
 590 the state-of-the-art practice (Figure 2).

591



592
 593 Figure 20 Histograms for RS and BS responses from MCS which considers possible measurement errors, and
 594 the corresponding measured vibration response.
 595

596 To quantify the HSI effect, the relative difference between the vibration responses is defined
 597 based again on Figure 2. Thus, for S2HI we have:

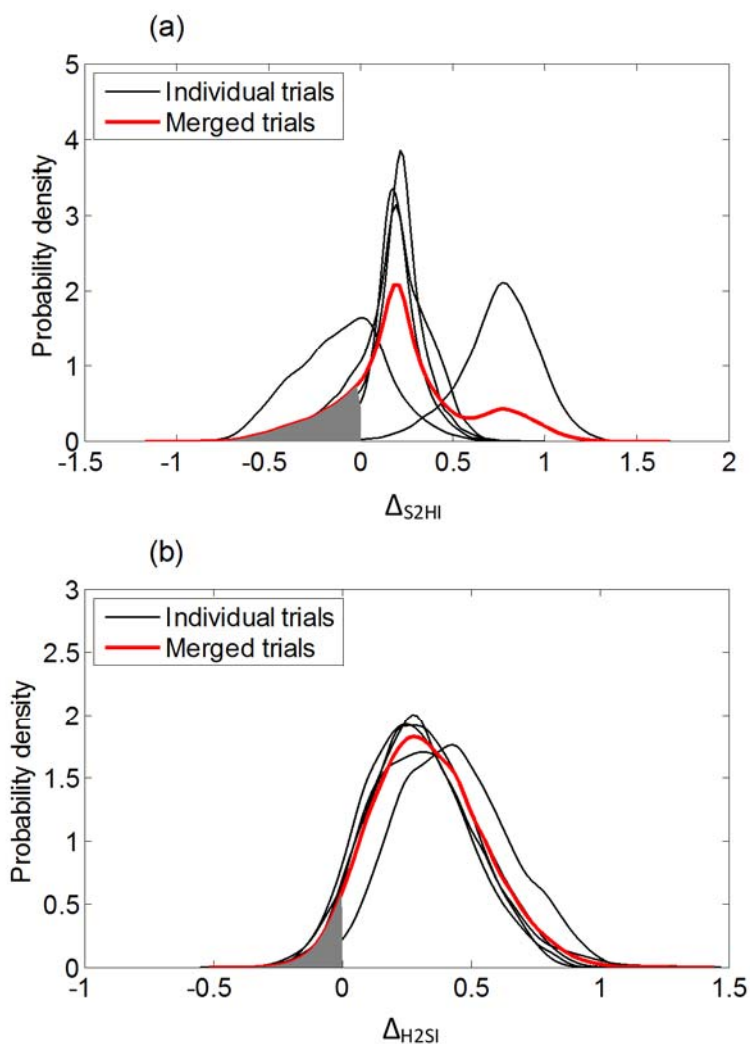
598
$$\Delta_{S2HI} = \frac{\mathbf{R}_{RS} - \mathbf{R}_{BS}}{R_M} \quad (11)$$

599 and for H2SI:

600
$$\Delta_{H2SI} = \frac{\mathbf{R}_{BS} - R_M}{R_M} \quad (12)$$

601 in which \mathbf{R}_{RS} and \mathbf{R}_{BS} are the vectors of simulated random responses for the RS and BS
 602 surfaces, respectively obtained from MCS. Then, PDFs are constructed for each trial
 603 individually, as well as for the group of 5 trials as a whole (merged trials). Figure 21 shows the
 604 PDFs for the exemplary test subject for each individual trial and the merged trials. It is clear

605 that most of the randomly realized Δ -values for both HSI forms are non-zero and positive,
 606 indicating the relative influence of HSI. The grey filled areas represent the probability of HSI
 607 non-existence or negative effect (negative side of the probability curves). In this example, this
 608 probability is 20% and 5% for S2HI and H2SI respectively, again reflecting that both are likely
 609 to exist and that H2SI is by far the stronger effect.



610 Figure 21 Probability density for the exemplary test subject at resonance for (a) S2HI (b) H2SI.
 611
 612
 613

614 The effects of both HSI forms on vibration response can be given as:
 615

616
$$R_M = \frac{R_{RS}}{1 + \Delta_{HSI}} \quad (13)$$

617 where,

$$618 \quad \Delta_{\text{HSI}} = \Delta_{\text{S2HI}} + \Delta_{\text{H2SI}} \quad (14)$$

619 The vibration response based on RS measurements is reduced by a factor to reach the measured
 620 vibration response. The most likely values of Δ_{S2HI} and Δ_{H2SI} are identified as the modes of
 621 the PDFs similar to Figure 21. These values are 0.21 and 0.27 for the exemplary test subject
 622 (Figure 21) giving a combined factor of 0.67 (as just one example). That is, the measured
 623 response is 67% of that estimated using rigid surface GRFs and a moving force numerical
 624 model (even allowing for amplitude-dependent damping). Table 6 shows these results for each
 625 test subject for the case at resonance only, since this is when HSI has most effect. The results
 626 show that HSI has a significant effect, and it increases with mass ratio. With further
 627 experiments, results of this nature could be used to provide more accurate vibration
 628 serviceability models that account for HSI.

629

630 Table 6. Relative and combined influence of HSI types (refer to equations (13) and (14)).

Test Subject	$\mu\mu\mu_m$ (%)	Δ_{S2HI}	Δ_{H2SI}	Δ_{HSI}	R_M/R_{RS}
1	0.33	0.03	0.02	0.05	0.95
2	0.40	0.03	0.04	0.07	0.93
3	0.50	0.12	0.17	0.29	0.77
4	0.60	0.21	0.27	0.48	0.67
5	0.70	0.10	0.28	0.38	0.72

631

632 **6. Conclusions**

633 In this paper, the human-structure interaction phenomenon was quantified using a novel
 634 experimental-numerical approach. The imparted footfall force to both rigid and bridge surface
 635 was measured along with the resulting bridge response. The moving force model was adopted
 636 to simulate vibration as a commonly-used model in design codes which ignores human-
 637 structure interaction. The difference between simulated and measured responses as well as the

638 difference between dynamic load factors of the forces on the rigid and bridge surface were used
639 as criteria to evaluate HSI existence.

640

641 It was found that human-structure dynamic interaction is associated both with the forces that
642 excite the structure (S2HI) and with the corresponding influence of humans on the dynamic
643 properties of the structure they occupy (H2SI). H2SI is found to be a far stronger influence than
644 S2HI for the bridge studied. The intensity of both S2HI and H2SI is found to increase as the
645 mass ratio between the human and structure increases. At resonance, where vibration amplitude
646 reaches its peak, the HSI effects are the most pronounced. The results of parametric statistical
647 hypothesis testing show that HSI is of statistical significance, and H2SI is very likely in
648 particular. Furthermore, non-parametric testing was done to see the effects of numerical model
649 and measurement errors on HSI existence. It shows that HSI remains of statistical significance
650 even accounting for numerical model and measurement errors. Similar to the parametric test,
651 it is found that H2SI is more statistically significant than S2HI. This approach enabled a
652 probabilistic quantification of both HSI effects, as well as their combined effect. Such an
653 approach could prove useful in adapting the moving force model to give results that compare
654 better to measurements.

655

656 The Warwick Bridge has a low pedestrian-to-bridge mass ratio, up to 0.7% in this study. For
657 bridges with higher mass ratios, the intensity of H2SI might be even more significant and
658 pedestrian effects on dynamic properties of the system could be even more pronounced than
659 bridge vibration effects on pedestrian walking force.

660

661 This study is a beneficial step forward towards quantifying HSI. It introduces a novel
662 framework which is a combination of an experimental and numerical approach to investigate

663 HSI. The findings provide a means of accounting for human-structure interaction. Such a
664 quantification of HSI could be incorporated into codes of practice rules to improve the accuracy
665 of vibration serviceability assessments.

666

667 **Acknowledgements**

668 This work was funded by a Monash-Warwick Alliance Seed Grant and a Monash Graduate
669 Scholarship (MGS).

670

671 **References**

- 672 [1] Živanović S, Pavic A, Reynolds P. Vibration serviceability of footbridges under human-
673 induced excitation: A literature review. *Journal of Sound and Vibration* 2005;279:1–74.
674 doi:10.1016/j.jsv.2004.01.019.
- 675 [2] Shahabpoor E, Pavic A, Racic V. Interaction between walking humans and structures in
676 vertical direction: a literature review. *Shock and Vibration* 2016;2016:12–7.
677 doi:10.1155/2016/3430285.
- 678 [3] Zammit G V., Menz HB, Munteanu SE. Reliability of the TekScan MatScan® system
679 for the measurement of plantar forces and pressures during barefoot level walking in
680 healthy adults. *Journal of Foot and Ankle Research* 2010;3:1–9. doi:10.1186/1757-
681 1146-3-11.
- 682 [4] Barnett S, Cunningham JL, West S. A Comparison of vertical force and temporal
683 parameters produced by an in-shoe pressure measuring system and a force platform -
684 Barnett.pdf 2001;16:353–7.
- 685 [5] Griffin MJ, Erdreich J. Handbook of human vibration. *The Journal of the Acoustical*
686 *Society of America* 1991;90:2213. doi:10.1121/1.401606.
- 687 [6] Cordero AF. Human gait, stumble and...fall? mechanical limitations of the recovery
688 from a stumble, University of Twente, Enschede, The Netherlands. 2003.
- 689 [7] McRobie A, Morgenthal G, Lasenby J, Ringer M. Section model tests on human-
690 structure lock-in. *ICE, Bridge Engineering* 2003;156:71–9.
- 691 [8] Blanchard J, Davies BL, Smith JW. Design criteria and analysis for dynamic loading of
692 footbridges. *Proceeding of a Symposium on Dynamic Behaviour of Bridges at the*
693 *Transport and Road Research Laboratory, Crowthorne, Berkshire, England, 1977.*
- 694 [9] P. Young. Improved floor vibration prediction methodologies, ARUP vibration seminar.
695 2001.
- 696 [10] Brownjohn JM., Pavic A, Omenzetter P. A spectral density approach for modelling
697 continuous vertical forces on pedestrian structures due to walking. *Canadian Journal of*
698 *Civil Engineering* 2004;31:65–77. doi:10.1139/103-072.
- 699 [11] Živanović S, Pavić A, Reynolds P. Probability-based prediction of multi-mode vibration
700 response to walking excitation. *Engineering Structures* 2007;29:942–54.
701 doi:10.1016/j.engstruct.2006.07.004.
- 702 [12] Piccardo G, Tubino F. Simplified procedures for vibration serviceability analysis of
703 footbridges subjected to realistic walking loads. *Computers and Structures*

- 2009;87:890–903. doi:10.1016/j.compstruc.2009.04.006.
- 705 [13] Venuti F, Racic V, Corbetta A. Modelling framework for dynamic interaction between
706 multiple pedestrians and vertical vibrations of footbridges. *Journal of Sound and*
707 *Vibration* 2016;379:245–63. doi:10.1016/j.jsv.2016.05.047.
- 708 [14] Racic V, Brownjohn JMW. Stochastic model of near-periodic vertical loads due to
709 humans walking. *Advanced Engineering Informatics* 2011;25:259–75.
710 doi:10.1016/j.aei.2010.07.004.
- 711 [15] Cross R. Standing, walking, running, and jumping on a force plate. *American Journal of*
712 *Physics* 1999;67:304. doi:10.1119/1.19253.
- 713 [16] Kram R, Griffin TM, Maxwell Donelan J, Hui Chang Y. Force treadmill for measuring
714 vertical and horizontal ground reaction forces. *Journal of Applied Physiology*
715 1998;7:764–9. doi:10.1016/j.jacr.2010.07.010.
- 716 [17] Weishaupt MA, Hogg HP, Wiestner T, Denoth J, Stüssi E, Auer JA. Instrumented
717 treadmill for measuring vertical ground reaction forces in horses. *American Journal of*
718 *Veterinary Research* 2002;63:520–7. doi:10.2460/ajvr.2002.63.520.
- 719 [18] Kluitenberg B, Bredeweg SW, Zijlstra S, Zijlstra W, Buist I. Comparison of vertical
720 ground reaction forces during overground and treadmill running. A validation study.
721 *BMC Musculoskeletal Disorders* 2012;13:235. doi:10.1186/1471-2474-13-235.
- 722 [19] Ohlsson SV. Floor vibrations and human discomfort, PhD Thesis, Gõteborg, Sweden.
723 Chalmers University of Technology, 1982.
- 724 [20] Pavic A, Yu CH, Brownjohn JMW, Reynolds P. Verification of the existence of human-
725 induced horizontal forces due to vertical jumping. *Proceedings of IMAC XX*, Vol. 1,
726 Los Angeles, CA, February 4–7, 2002, p. 120–6.
- 727 [21] Van Nimmen K, Lombaert G, Jonkers I, De Roeck G, Van Den Broeck P.
728 Characterisation of walking loads by 3D inertial motion tracking. *Journal of Sound and*
729 *Vibration* 2014;333:5212–26. doi:10.1016/j.jsv.2014.05.022.
- 730 [22] Bocian M, Brownjohn JMW, Racic V, Hester D, Quattrone A, Monnickendam R. A
731 framework for experimental determination of localised vertical pedestrian forces on full-
732 scale structures using wireless attitude and heading reference systems. *Journal of Sound*
733 *and Vibration* 2016;376:217–43. doi:10.1016/j.jsv.2016.05.010.
- 734 [23] Dang HV, Živanovic S. Influence of low-frequency vertical vibration on walking
735 locomotion. *Journal of Structural Engineering* 2016;142:1–12.
736 doi:10.1061/(ASCE)ST.1943-541X.0001599.
- 737 [24] Caprani CC, Ahmadi E. Formulation of human-structure system models for vertical
738 vibration. *Journal of Sound and Vibration* 2016.
739 doi:http://dx.doi.org/10.1016/j.jsv.2016.05.015.
- 740 [25] Busca G, Cappellini A, Manzoni S, Tarabini M, Vanali M. Quantification of changes in
741 modal parameters due to the presence of passive people on a slender structure. *Journal*
742 *of Sound and Vibration* 2014;333:5641–52. doi:10.1016/j.jsv.2014.06.003.
- 743 [26] Ahmadi E, Caprani CC, Heidarpour A. An equivalent moving force model for
744 consideration of human-structure interaction. *Applied Mathematical Modelling*
745 2017;51:526–45. doi:10.1016/j.apm.2017.06.042.
- 746 [27] Willford M. Dynamic actions and reactions of pedestrians. *Proceedings of the*
747 *International Conference on the Design and Dynamic Behaviour of Footbridges*, Paris,
748 France: 2002, p. 66–73.
- 749 [28] Živanović S, Diaz IM, Pavić A. Influence of walking and standing crowds on structural
750 dynamic properties. the 27th IMAC Conference, Orlando, USA: 2009.
- 751 [29] Nimmen K Van, Maes K, Živanović S, Lombaert G, Roeck G De, Broeck P Van den.
752 Identification and modelling of vertical human-structure interaction. *Proceedings of the*
753 *33th International Modal Analysis Conference Series*, Orlando: 2015.

- 754 [30] Živanović S, Pavić A, Ingólfsson ET. Modeling spatially unrestricted pedestrian traffic
755 on footbridges. *Journal of Structural Engineering* 2010;136:1296–308.
756 doi:10.1061/(ASCE)ST.1943-541X.0000226.
- 757 [31] Caprani CC, Keogh J, Archbold P, Fanning P. Enhancement factors for the vertical
758 response of footbridges subjected to stochastic crowd loading. *Computers and Structures*
759 2012;102–103:87–96. doi:10.1016/j.compstruc.2012.03.006.
- 760 [32] Kasperski M. Damping induced by pedestrians. the 9th International Conference on
761 Structural Dynamics, EUROLYN, Porto, Portugal: 2014, p. 1059–64.
- 762 [33] OHBDC, Ontario Highway Bridge Design Code, Highway Engineering Division,
763 Ministry of Transportation and Communication, Ontario, Canada. 1983.
- 764 [34] BSI (British Standards Institution). U.K. national annex to Euro- code 1: Actions on
765 structures—Part 2: Traffic loads on bridges. EN 1991-2:2003, London. 2008.
- 766 [35] ISO 10137 - Bases for design of structures - Serviceability of buildings and walkways
767 against vibrations. 1992.
- 768 [36] Eurocode 5, Design of Timber Structures—Part 2: Bridges, ENV 1995-2: 1997, European
769 Committee for Standardization 1997.
- 770 [37] Sétra, Guide méthodologique passerelles piétonnes (Technical guide Footbridges:
771 assessment of vibrational behaviour of footbridges under pedestrian loading). 2006.
- 772 [38] Design of footbridges – HIVOSS (Human Induced Vibrations of Steel Structures). 2009.
- 773 [39] Lasheen MRM, Zivanovic S, Salem E, Dang H V. Static and dynamic performance of a
774 steel-concrete composite bridge. The 9th International Conference on Structural
775 Dynamics, EUROLYN, 2014, p. 1007–12.
- 776 [40] Forner Cordero A, Koopman HJFM, Van Der Helm FCT. Use of pressure insoles to
777 calculate the complete ground reaction forces. *Journal of Biomechanics* 2004;37:1427–
778 32. doi:10.1016/j.jbiomech.2003.12.016.
- 779 [41] Fong DTP, Chan YY, Hong Y, Yung PSH, Fung KY, Chan KM. Estimating the
780 complete ground reaction forces with pressure insoles in walking. *Journal of*
781 *Biomechanics* 2008;41:2597–601. doi:10.1016/j.jbiomech.2008.05.007.
- 782 [42] Tekscan, Force Measurement and Tactile Sensors, 2017. <https://www.tekscan.com>.
- 783 [43] Bendat JS, Piersol AG. Random data: analysis and measurement procedures. Wiley
784 Series in Probability and Statistics; 2009.
- 785 [44] Caprani CC. A modal precise integration method for the calculation of footbridge
786 vibration response. *Computers and Structures* 2013;128:116–27.
787 doi:10.1016/j.compstruc.2013.06.006.
- 788 [45] Racic V, Brownjohn JMW. Mathematical modelling of random narrow band lateral
789 excitation of footbridges due to pedestrians walking. *Computers & Structures*
790 2012;90:116–30. doi:10.1016/j.compstruc.2011.10.002.
- 791 [46] Kerr SC. Human Induced Loading on Staircases. 1998. doi:10.1016/S0141-
792 0296(00)00020-1.
- 793 [47] Bocian M, Macdonald JHG, Burn JF. Biomechanically inspired modeling of pedestrian-
794 induced vertical self-excited forces. *Journal of Bridge Engineering* 2013;18:1336–46.
795 doi:10.1061/(ASCE)BE.1943-5592.0000490.
- 796 [48] Shahabpoor E, Pavic A, Racic V, Zivanovic S. Effect of group walking traffic on
797 dynamic properties of pedestrian structures. *Journal of Sound and Vibration*
798 2017;387:207–25. doi:10.1016/j.jsv.2016.10.017.
- 799 [49] Živanović S, Johnson RP, Dang H V., Dobrić J. Design and construction of a very lively
800 bridge. In: Topics in Dynamics of Civil Structures, Volume 4. Conference Proceedings
801 of the Society for Experimental Mechanics Series., Springer, New York, NY; 2013, p.
802 371–80. doi:10.1007/978-1-4614-6555-3_41.
- 803 [50] Johnson O. Information theory and the central limit theorem. Imperial College Press;

- 804 2004.
805 [51] Chen SX. Probability density function estimation using gamma kernels. *Annals of the*
806 *Institute of Statistical Mathematics* 2000;52:471–80. doi:10.1023/A:1004165218295.
807